Ultrafast Interfacial Proton-Coupled Electron Transfer

Hrvoje Petek*,† and Jin Zhao†,‡

Department of Physics and Astronomy, University of Pittsburgh, Pittsburgh Pennsylvania 15260, United States, and Hefei National Laboratory for Physical Sciences at Microscale, University of Science and Technology of China, Hefei, Anhui, China

Received May 25, 2010

Contents

Hrvoje Petek studied molecular spectroscopy with R. W. Field as an undergraduate student at MIT and with C. B. Moore as a graduate student at U. C. Berkeley. After obtaining his Ph.D. degree in 1985, he joined the group of K. Yoshihara as a postdoctoral fellow and a Research Associate at the Institute for Molecular Science, where he mastered the arts of ultrafast spectroscopy. Later as a Group Leader at Hitachi Advanced Research Laboratory, he brought these skills to studies of ultrafast surface dynamics. In 2000, he became a Professor of Physics, and in 2002 a Professor of Chemistry at the University of Pittsburgh, where he is also the co-Director of the Petersen Institute for NanoScience and Engineering. He employs ultrafast photoelectron spectroscopy and microscopy, and theory to study electron and nuclear dynamics of clean and molecule covered metal and semiconductor surfaces, with a particular focus on photocatalysis. Petek was an Alexander von Humboldt Senior Scholar and is a Fellow of the American Physical Society. Since 2006, he has been the Editor-in-Chief of Progress in Surface Science.

1. Introduction

Considering how pervasive charge transfer (CT) processes are in heterogeneous media, proton-coupled electron transfer (PCET), in its many different manifestations, is undoubtedly one of the most important interfacial chemical processes.[1−4] Charge transport plays a central role in a variety of energy transduction processes in biological and artificial photosynthetic systems. For instance, proton pumping in biological membranes serves to establish an electrochemical potential that enables conversion of light into chemical energy. Whereas a variety of spectroscopic and microscopic methods are enabling steady progress in unraveling of photobiological charge transduction,[5−7] our atomistic understanding of even the seemingly simplest interfacial processes, for example the adsorption and evolution of H_2 molecules at a Pt electrode−H_2O liquid interface (e.g., the Heyrovsky reaction: $H_2 \rightarrow H_{ad} + H^+ + e^-$)[8,9] or even the discharge of H^+ at water−metal interfaces (Volmer reaction $H^+ + e^- \rightarrow H_{ad}$)[9,10] remains at a primitive level, in part because of the difficulty of probing ultrafast CT processes at solid−liquid interfaces.

Interfacial reduction/oxidation processes in the presence of applied electrical potential or induced by electron−hole pair excitation in a solid typically involve multiple electron, proton, or hydrogen atom transfer steps, which can happen in different sequences or in a concerted manner with different, pathway-dependent energy costs or gains. Although we can propose schemes for heterogeneous chemical processes, such as for solar energy conversion through the photocatalytic splitting of H_2O, the reduction of CO_2 into chemical feedstocks and fuels (e.g., Scheme 1),[11,12] or the photocatalytic mineralization of harmful organic compounds,[13] such schemes provide very little insight into the atomic scale processes, the energetic hypersurfaces, or the dynamical time scales for the individual steps. Most importantly, such processes occur at a solid electrode−solvent

* Author to whom correspondence should be addressed. E-mail address: petek@pitt.edu.
† University of Pittsburgh.
‡ University of Science and Technology of China.

10.1021/cr1001595
Published on Web 11/09/2010

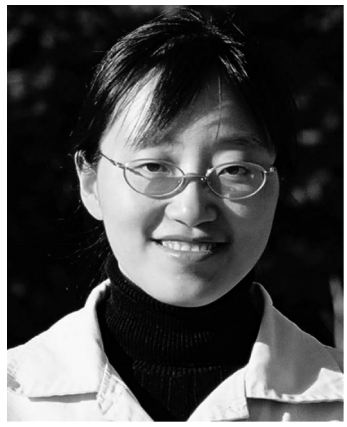

Jin Zhao received her B.S. degree from University of Science and Technology of China (USTC) in physics in 1998. After that she completed her Ph.D. work with Prof. J. G. Hou and Prof. Jinlong Yang in 2003 in USTC. For the Ph.D. degree she mainly worked on theoretical research of the electronic properties of small molecules and nanoclusters with cooperation with STM experiments. In March 2004, she joined the research group of Prof. Hrvoje Petek at the University of Pittsburgh. In March 2010, she returned to USTC as a Professor. The focus of her research is theoretical research on the electronic structure and dynamics of excited electrons in different materials.

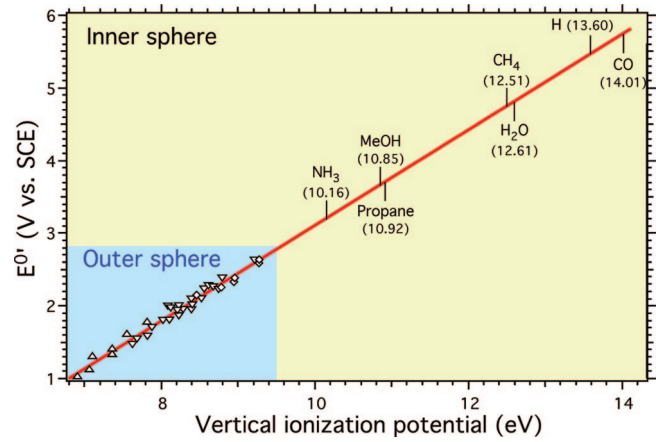

Figure 1. Correlation of electrochemical standard potential $E^{\circ\prime}$ vs vertical ionization potential for a series of aromatic compounds that have been measured in acetonitrile solution, and extrapolation of the trend to several other prototypical molecules with ionization potentials that exceed 10 eV.[15,16] The electron transfer from the compounds within the blue box can occur through an outer sphere process, whereas the high ionization potential compounds can react only through an inner sphere electrocatalytic process because at the implied electrochemical potentials the solvent would undergo electron transfer in preference to the solute.

interface, but the solvent is missing in accounting for the elementary steps. Our intuition and experience of homogeneous processes, however, demand that these processes occur through intimate correlation of light particle (electron and proton) motion on potential hypersurfaces that are established by the heavy particle motions of the solvent molecules and substrate atoms and are subject to thermally induced fluctuations.

The energy and charge transduction processes usually occur through transport of light particles through highly inhomogeneous environments. Unlike the homogeneous PCET, electrons and protons transfer between donors and acceptors in profoundly different media; electrons transfer between the delocalized bands of a crystalline solid and the localized state defined by the corrugated energy landscape of a molecular liquid with local order established through weak molecular interactions, e.g., a hydrogen-bonding network, whereas protons migrate between the hydrogen bonding network of liquid and well-defined sites on an atomically ordered electrode surface. Moreover, charges are subject to a strong gradient in the interfacial potential that arises from the difference in binding energies with respect to the vacuum level of the solid and liquid media, and they can be modified with an externally applied potential. In response to the potential discontinuity, electrons in the electrode surface and molecules and ions in the liquid form the capacitive electrical double (Helmholtz) layer at the interface between the regions of constant potentials within the solid electrode and bulk solvent.

Scheme 1

$$2H^+ + 2e^- \rightarrow H_2$$

$$H_2O \rightarrow {}^1/_2O_2 + 2H^+ + 2e^-$$

$$CO_2 + e^- \rightarrow CO_2^{\bullet -}$$

$$CO_2 + H^+ + 2e^- \rightarrow HCO_2^{\bullet -}$$

$$CO_2 + 2H^+ + 2e^- \rightarrow CO + H_2O$$

$$CO_2 + 4H^+ + 4e^- \rightarrow HCOH + H_2O$$

$$CO_2 + 6H^+ + 6e^- \rightarrow CH_3OH + H_2O$$

$$CO_2 + 8H^+ + 8e^- \rightarrow CH_4 + 2H_2O$$

Contrary to the reductionism in Scheme 1, electrons and protons at a solid−liquid interface never appear or evolve in their bare form. Rather, dynamic polarization of free and bound electrons and nuclear motions of lattice ions and solvent molecules in the interfacial region screen their Coulomb potentials on time scales that span a range from attoseconds to as long as one is willing to wait.[14] The transmission of charges through the interfacial region occurs with a cost or gain in energy associated with screening of the bare particles on either side of the interface, and the work associated with charge transport across the interfacial potential gradient. The interfacial CT may occur adiabatically, with the charged particles responding to the motion of heavy nuclei, or nonadiabatically, such as when photon excitation induces CT from one to the other side of the interface. The energy cost for charge transfer across an interface with respect to the potentials of reactants and products within each medium appears in overpotentials for driving the electrochemical process. Efficient energy conversion by an artificial photocatalytic process such as in Scheme 1 requires an intimate understanding and control of multiple correlated CT steps with minimal loss of efficiency through competing chemical processes and frictional losses. Correlated interfacial transduction of electrons and protons offers the possibility of greater efficiency and lower activation barriers than uncorrelated processes. Of particular interest in many practical applications and biological processes is the movement of charge across the water interface with solids and biological materials.

We can separate the discussion of interfacial PCET into the inner Helmholtz layer and outer layer interactions, as done recently by Bard in a discussion of electrocatalytic and photocatalytic chemistry.[15] Figure 1 shows the correlation

between standard electrochemical potentials vs the vertical ionization potentials for a series of solution species.[15,16] The ionization potentials within the blue box are sufficiently low for ET to occur as an outer sphere process within a solvent such as acetonitrile. For high ionization potential substances, however, electrochemical reduction can only occur as an inner sphere process involving electrocatalysis or photocatalysis, because the solvent would be reduced at a lower potential than the substance of interest. Therefore, many processes that are central to clean energy generation can only be achieved as inner sphere processes where specific adsorbate−substrate interactions can lower the activation energy for interfacial ET.[17] Moreover, of particular interest here is how to couple the electron and proton transfer dynamics as a strategy for lowering the energetic cost in interfacial energy transduction processes.

A significant difference between homogeneous and heterogeneous PCET, particularly for inner sphere processes, is the coupling of electrons to the electronic continua of semiconductor or metal electrodes. The electronic band widths of the valence and conduction bands of solids are typically several electronvolts. The coupling strengths increase exponentially with the proximity to surfaces. Because of the broken symmetry at interfaces, the screening efficiency of solvent molecules is also diminished within the inner Helmholtz layer, where the interfacial potential gradient and electronic coupling are the largest.[18] Thus, for the inner shell interactions, where adsorbates are in direct contact with substrate, the coupling strengths tend to be the dominant factor that defines the CT dynamics. The coupling strengths of electronically excited states of chemisorbed atoms and molecules in resonance with the unoccupied delocalized states of the substrates can be estimated from resonance line widths based on the energy−time uncertainty principle.[19,20] In the absence of the more definitive time domain measurements,[21] line widths in surface electronic spectra provide a measure of interfacial ET time scales at metal surfaces in a few hundred attosecond to few tens of femtosecond range.[22] These time scales are generally faster than the ballistic solvent response to suddenly changing charge distributions.[23,24] For the strong inner shell coupling, it is hardly appropriate to describe the PCET dynamics in terms of weakly coupled Marcus−Jortner parabolas,[25,26] such as employed for other media elsewhere in this Special Issue on PCET dynamics. The widths of transiently occupied resonances in photoinduced surface processes, however, strongly depend on the band structure of the substrate and how the electron density is distributed on an adsorbed atom or molecule with respect to the substrate.[21,22,27,28] Thus, it is also possible to find adsorbate/substrate systems where photoexcitation-induced nuclear wave packet motion of adsorbate can compete with and even suppress the competing interfacial ET process.[29,30]

The recently developed theories of interfacial PCET are predicated[25,31−34] on the near thermal equilibrium and intermediate to weak coupling that follows from screening of interfacial charges within the outer Helmholtz layer. For outer shell interactions, where an intervening solvent layer prevents the direct coupling, charge transfer has to occur through the inner shell layer. Under such circumstances, the situation is more comparable to the homogeneous case, where the solvent reorganization energy can be the controlling factor for CT dynamics.[31] Because of their very high vibrational frequencies and incomplete screening of the proton charge in both the covalent and hydrogen bonded situations, H atoms can be very effective in solvating the transient interfacial electron distributions. The excess charge at an interface can be stabilized effectively through the solvent reorganization even if the interfacial molecular overlayer is only three monolayers (ML) thick. For example, electrons injected into the conduction band of an H_2O ice film on metal surfaces decay on the femtosecond time scale, but trapping and partial solvation by the reorganization of water molecule structure at the water−air interface can increase their lifetimes to minutes.[14,35,36] Such dramatic stabilization arises from the large solvent reorganization energy for back ET into the substrate and low tunneling probability through the dielectric medium. Thus, the dynamic response of an interface, which intimately depends on the solvent−substrate interaction, can effectively quench CT through the inertial solvent reorganization.

Because very few experiments have probed interfacial PECT dynamics and our understanding is mainly confined to the measurements of an overall kinetic process leading to stable reaction products with quantifiable yields, from which we can only hypothesize about the key mechanistic steps and reaction intermediates, we wish to motivate a more compete understanding of surface chemical reactions at the level of dynamics of chemical bond breaking and making, in particular, in terms of the forces acting on the coupled proton and electron motions during a chemical transformation. Therefore, we wish the reader to consider this article as a preview rather than a review. We aim to present a glimpse of ultrafast dynamical processes involved in interfacial PCET based on well-documented examples from the surface science literature. We take a catholic perspective of PCET in order to include several regimes involving different degrees of coupling strengths and solvation energies that can account for dynamics spanning more than 15 orders-of-magnitude in time. In the following sections we introduce the electronic properties of metal−molecule interfaces; then we introduce PCET dynamics in the strong coupling regime, as represented by photoinduced C−H bond dissociation of alkanes; next we describe our experimental and theoretical studies of PCET in the intermediate coupling regime for CH_3OH covered rutile $TiO_2(110)$ surfaces; and finally, we provide perspectives for the future of interfacial PCET dynamics.

2. Electrical Potential of a Chemisorption Interface

A particular aspect of interfacial CT is the sharp potential discontinuity at a metal−molecule junction that can provide the driving force or a barrier for the charge transport across an electrochemical interface. How the molecular reactant and product energy levels align with respect to the Fermi level (E_F) of the metal at small enough distances to allow the interfacial CT processes to proceed determines whether such process are exo- or endothermic. Differences in material specific electron binding energies with respect to the common reference energy of a free electron at rest in the vacuum (the vacuum level, E_{vac}) between solid electrode and molecular phases cause a potential step in traversing their interface. The actual discontinuity at the interface is defined by the difference in the potentials in the two phases, the interface charging and CT when the two substances are placed into mutual contact, and the polarization created by an externally applied potential. The potential step gives rise to a surface dipole field, known as the Helmholtz or electrical double layer (DL), that forms through charging of the electrode and

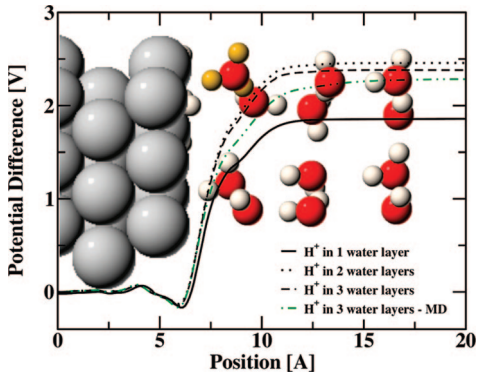

Figure 2. Structure of a Pt(111) surface terminated by H atoms and in contact with 3 ML of H_2O from a molecular dynamics simulation.[8] The potentials for various H_2O coverages and from MD simulation show the potential discontinuity a positive charge would experience on crossing the solid−liquid interface, assuming the liquid does not rearrange to solvate the charge. Reprinted with permission from ref 8. Copyright 2008 Elsevier.

the screening of this surface charge by adsorption and polarization of ions and molecules of the electrolyte.[8,37−42] According to the Helmholtz and Gouy−Chapman theories of the electrical DL,[37,38] the surface molecules and ions (if present) arrange at the interface to screen the surface electric field, which can be as high as 1 V/Å. As an example, Figure 2 shows the calculated potential jump for a positive test charge at a charged H_2O−Pt(111) interface.[8] The interfacial electric field is established by H atoms, which partially transfer their electrons to a Pt electrode, leaving the surface protons to be partially solvated by proximate water molecules. Screening of the interfacial field occurs within the Debye length sale, which is 0.7 nm for water at room temperature.[43] Interfacial PCET typically occurs within or through the DL; therefore, it is essential to incorporate both the interfacial field gradient and the atomistic description of the DL structure in describing heterogeneous PCET processes.[44] In an electrochemical system, an externally applied potential provides a continuously tunable parameter that can be used to modify the interfacial potential step and chemical composition and, thereby, to control the interfacial structure and, consequently, the CT processes.[25,31−34]

We chose, however, to elaborate interfacial PCET from a more atomistic perspective than the capacitive interfacial DL model. Our examples will be based on surface science studies where the heterogeneous PCET interface consists of a single crystal metal or semiconductor surface covered by a fraction to a few atomic or molecular monolayers (ML) of adsorbates, and ultrafast laser excitation creates a perturbation in the interfacial charge distribution, generating forces that drive proton or H atom motion. Under these circumstances, DL is only partially formed and the electrical potential in the molecular layer is strongly surface and adsorbate structure dependent. The interfacial structure is defined by specific surface−molecule interactions, which can often be stronger than the molecule−molecule interactions within the molecular layer.[45] Therefore, it is more useful to describe the interface through specific chemical interactions, which define the interfacial molecular and electronic structure. The chemical and electrostatic descriptions of an interface should, of course, be self-consistently defined by the same molecule−surface and molecule−molecule interactions.[46]

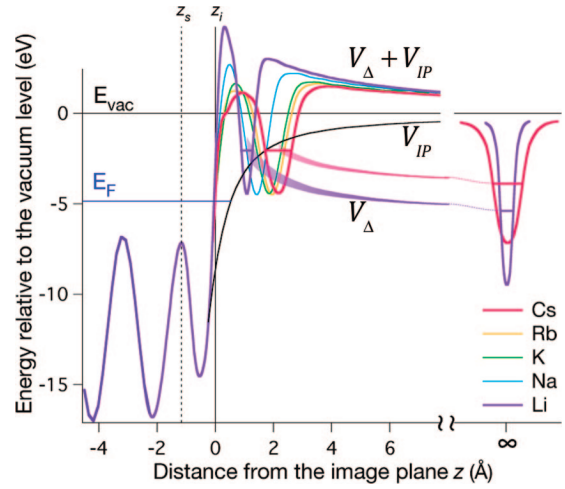

Figure 3. Effective potential for a negative test charge for an alkali atom (Li−Cs) at its chemisorption height above a Cu(111) surface, as a function of distance z from the image plane, z_i.[27] The effective potential is constructed from the model potential of Cu(111), including the image potential tail V_{IP} at the surface (black line), the alkali atom pseudopotential as a free atom ($z = \infty$), and their main mode of interaction through the image charge repulsion V_Δ. z_s locates the edge of the top surface layer, and the horizontal lines for Li and Cs indicate the 2s and 6s level energies of the free and chemisorbed atoms. Reprinted with permission from ref 27. Copyright 2008 American Physical Society.

2.1. Electron Potential of an Alkali Atom−Metal Interface

We begin our exposition with a description of the potential of a metal−vacuum interface. Surface science studies provide detailed information on molecule−surface interactions that define the interfacial potential.[27,47,48] Although our discussion will mostly focus on metals, qualitatively similar potentials are to be expected for other materials, with differences appearing in material-specific screening properties and the nature of adsorbate−surface bonding.[49] Through polarization of the free and bound electrons in a metal, the potential of an external charge induces a screening charge in front of a metal surface.[50,51] The effect of the induced charge can be represented by a fictitious "image" charge of the opposite sign that can be thought of being located within metal at the position of the mirror image of the external charge with respect to an image plane.[52] The resulting attractive Coulomb potential between the external and image charges has a $-1/4z$ dependence on the distance z from the image plane. The image plane is located typically ~1 Å outside the center of the terminal surface atomic layer, as shown in Figure 3, and it has been tabulated for many metal surfaces as a parameter that interpolates the electronic potential between the vacuum and bulk limiting forms.[53,54] The image potential supports a Rydberg-like series of image potential (IP) surface states that asymptotically converge in the limit of large principal quantum number n to E_{vac}. The structure and dynamics of these IP states on bare and molecule covered metal surfaces have been the subject of intense investigations by time-resolved two-photon photoemission (TR-2PP) spectroscopy and theory, because they provide incisive information on the interfacial potential and dynamics of the interfacial electron scattering processes involved in the electron energy relaxation, trapping, and transport.[35,36,55−57]

In addition to the image potential, the full potential that governs the transport of electrons through a metal−adsorbate−vacuum interface, such as depicted in Figure 3

for alkali atoms chemisorbed on a Cu(111) surface, includes the crystal potential of the solid, which can be reasonably described by density functional theory (DFT). *Ab initio* descriptions of the image potential, however, require approaches beyond DFT such as the many-body perturbation theory.[58,59] Alternatively, the electronic structure of many metals can be represented by empirical one-dimensional potentials that have been parametrized to provide accurate values for the band dispersions and projected band gaps of the bulk electronic structure and the surface electronic states that exist within the band gaps, including the IP states.[27,53,54,60]

The image charge interaction also describes the stabilization of the electron and hole acceptor states of molecules at or near surfaces. When an electron is removed from the HOMO of a molecule to generate a cation or is added to the LUMO to form an anion, as would be the case in charge transport through a metal−molecule interface, or in measuring photoemission or inverse photoemission spectra, the corresponding ionic states are stabilized by polarization of a metal surface with respect to the corresponding states of the isolated molecule. Specifically, when chemical interactions can be neglected because of the nature of molecule−surface interaction or when the distance is sufficiently large to preclude covalent bonding, the image charge interaction shifts the HOMO states upward and the LUMO states downward with $^1/_{4z}$ dependence, with the net effect of decreasing the HOMO−LUMO gap by $^1/_{2z}$.[27,58,59,61]

Unless chemical interactions dominate, the image charge interaction provides an accurate description of the perturbation of the adsorbate electronic structure in the presence of the Fermi sea of the metal substrate for a broad range of atomic and molecular adsorbates.[27] The image charge interaction provides a predictive model of the surface electronic structure in the case of strong ionic bonding or weak chemisorption, i.e. when the HOMO and LUMO orbitals are localized on the adsorbates rather than being shared in a covalent bond.[27,62,63] For instance, the energies of the unoccupied states of the alkali and alkaline earth atoms chemisorbed on noble metal surfaces this model obtains are in near-quantitative agreement with more rigorous theoretical methods and with measurements by two-photon photoemission (2PP) spectroscopy.[27,28,64] The model also works for weakly interacting species, such as the layer thickness dependent core and valence level binding energies of physisorbed rare gas atoms or molecules on metals.[62,63]

As an example of how the image charge interaction affects interfacial potentials, in Figure 3 we reproduce the potentials that would be experienced by a negative test charge as it is transported through the vacuum interface of a single alkali atom on a Cu(111) surface.[60,61] The effective potentials are assembled from those of the noninteracting metal surface and free alkali atom, and their perturbation through the image charge interaction.[65] The interaction of the *n*s valence electron of an alkali atom (i.e., HOMO level) with a metal surface can be decomposed into the image charge attraction to its own image charge ($V_{IP} = -^1/_{4z}$ potential) and repulsion from the negative image charge of the positive alkali atom core ($V_\Delta = +^1/_{2z}$ potential for an electron orbital centered on the ionic core). The net interaction destabilizes the *n*s electron level with a $V_{IP} + V_\Delta = +^1/_{4z}$ dependence. Therefore, as z is decreased from infinity to the bonding distance, the *n*s levels of alkali group atoms are destabilized to ∼1.9 eV below E_{vac} with respect to their unperturbed energies, as given by their ionization potentials of 3.9−5.4 eV relative to E_{vac} for Cs to Li.[27,66] For the Li atom, which has the shortest atom−surface bonding distance, the repulsion destabilizes its 2s level by ∼3.5 eV, whereas, for the much larger Cs atom, the 6s level is destabilized by only 2 eV. Because the *n*s levels are lifted above E_F, they become unoccupied resonances in the surface density of states (DOS). The effective electron potentials that have been derived according to the above prescription are validated by 2PP measurements on alkali and alkaline earth atom covered metal surfaces, which find excellent agreement between the experimentally measured and calculated energies of the *n*s state derived σ resonances.[27,64] Having transferred their valence electron, the positive alkali atom cores are bound by the Coulomb potential to their image charges in the substrate, in an analogous manner to ions in a DL at a metal−electrolyte interface. At larger alkali atom coverages, the formation of a surface dipole field, associated with alkali ions and their negative image charges, stabilizes the σ resonance energy; this effect of surface dipoles is well established in the field of molecular electronics.[67,68] At coverages approaching 1 ML, dipole−dipole depolarization causes repopulation of the σ resonance and ionic-to-metallic transition of the overlayer film.[69]

2.2. Hydrogen Atom−Metal Surface Interactions

Based on the above concept of formation of the interfacial electronic structure, next we consider the potential of the first member of the alkali atom group, namely an H atom or a proton in front of a metal surface in a vacuum and when solvated in, e.g., H_2O. Like an electron, a bare proton in a vacuum will experience the attractive $-^1/_{4z}$ potential of its image charge. At a sufficiently large distance above a metal, we can regard the interaction of the H atom just as we did the other members of the alkali atom group: the 1s electron will experience the same net repulsive $+^1/_{4z}$ potential. The unscreened Coulomb interaction between electron and proton makes the ionization potential of the 1s electron of the H atom (13.6 eV) much higher than those of alkali atoms. Because the screened Coulomb interaction between an electron and its image charge in a metal is weaker by a factor of $\sim^1/_{16}$ than the bare interaction between an electron and proton,[70] the image charge repulsion cannot destabilize the 1s electron sufficiently to raise it above E_F.[70] Therefore, in contrast to alkali atoms, H atoms chemisorb on metals by forming a covalent bond, which is particularly favorable for metals with d-bands near the Fermi level.[9] Even though the energy of the 1s state is below E_F, strong interactions with the d-band of the substrate can induce broadening, allowing partial charge transfer to occur.[9] The charge separation between surface protons and metal electrons, however, is never as complete as for alkali atoms on metals. The interfacial potential in Figure 2 reflects this charge polarization in the presence of water molecules, which solvate the surface adsorbates and define the dielectric environment of the molecular phase.

The interfacial potential for the Volmer reaction ($H_{(s)} \rightarrow H^+_{(aq)} + e^-_{(m)}$), i.e. the discharge of a proton at a metal surface, is considerably modified from the vacuum case by the presence of a solvent such as H_2O. The Volmer reaction has been investigated for various model structures for the H and H^+ reactant/product solvation shells at different levels of theory.[9,18,71,72] The solvent profoundly alters the interaction of the H atom with metals by stabilizing H^+ by ∼11 eV with respect to E_{vac} through solvation.[40,73−75] In liquid water,

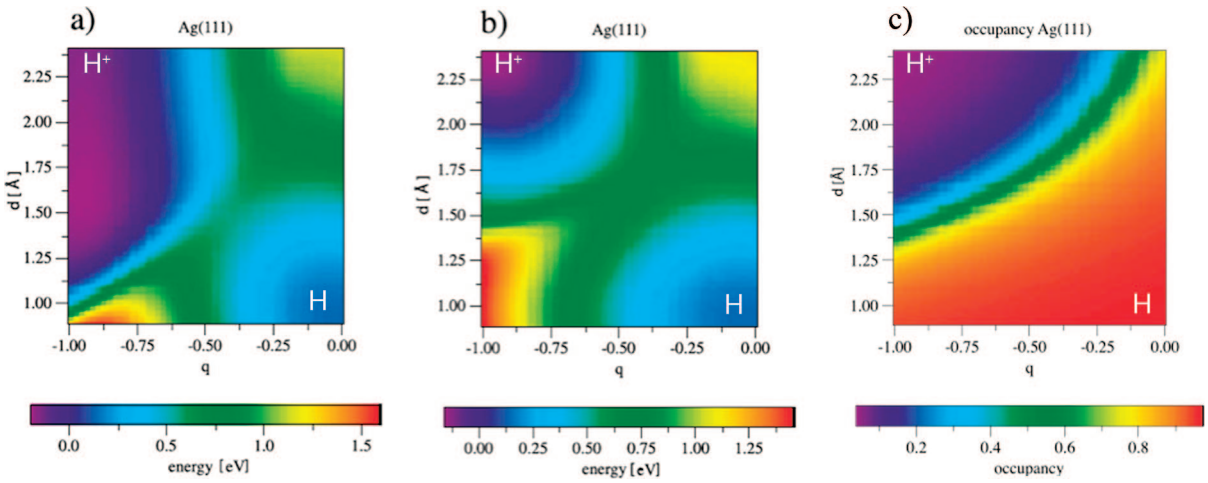

Figure 4. (a and b) Free energy surfaces for hydrogen adsorption on Ag(111) plotted against the H/H$^+$ distance from the Ag surface (d), and normalized solvent coordinate (q), where $q = 0$ corresponds to a discharged H atom and $q = -1$ to the solvated proton. In part a the solvent reorganization energy is held constant at 3 eV, whereas in part b, on account of desolvation, it decreases as solvated proton approaches the surface. The respective activation energies for H atom discharge are 0.57 and 0.71 eV for parts a and b. (c) Occupancy of the hydrogen 1s state as a function of the same coordinates.[18] Reprinted with permission from ref 18. Copyright 2009 American Physical Society.

H^+ is solvated in the putative ideal Eigen [$H_3O^+ \cdot (H_2O)_3$] or Zundel ($H_5O_2^+$) solvation structures.[76,77] A proton in water is never a well-defined species because of the rapid exchange with hydrogen atoms bound to the same or neighboring O atoms. For a proton to transfer between the solvent environment and its chemisorption site on a metal surface in contact with the solvent requires interfacial electron transfer and substantial solvent reorganization associated with the charge redistribution.[25,78] Schmickler and co-workers have devised a model for the electrochemical charge transfer processes involved in the Volmer reaction by representing different stationary states that are coupled by either proton or electron transfer with Marcus parabolas and employing a second quantized Hamiltonian to model the individual transfer processes and the coupling with the solvent.[18] More realistic models by the same group, such as shown in Figure 4, describe how in the interfacial region the potential landscape is influenced by a partial desolvation as a proton emerges from the bulk solvent onto the interface. The potentials for proton transfer to a metal surface and for electron transfer from a metal to form a chemisorbed H atom are defined by the undressing of the proton solvation shell in the interfacial region and the correlated polarization of the metal substrate.[18] The thermodynamic driving force, which determines the course of H atom adsorption, is given by the solvation energy of a proton, the work function of a metal, and the interfacial potential, which can be externally controlled.[40,75] The overpotential for the process, however, is intimately related with the energetic barriers associated with the interfacial proton and electron transfer processes,[9,18,71] with the possibility of PCET providing the lowest energy pathway.

Unfortunately, the atomistic understanding of fundamentally important processes such as the Volmer reaction is only available from sophisticated theoretical calculations on model systems that can strive to capture the essential complexity of the molecule−metal interface at finite temperatures. For instance, Wilhelm et al. have performed molecular dynamics (MD) simulations on the discharge of H^+ at the Pt(111) surface by representing the solvated ion complex by two water molecules and a proton forming the Zundel structure (Figure 5a) and parametrizing the potential energy surfaces through an empirical valence bond model.[71] In the MD simulations, the positive charge diffuses within the Zundel structure in a Grotthuss-like manner until it is transferred to the first layer molecule, where a proton may already be facing the surface. Depending on the Pt−O distance, the potential energy surface may or may not have a barrier to proton discharge. The MD trajectory in Figure 5b captures the candidate H atom as it localizes in the first layer water 2.5−3.0 Å above a Pt atom, and as it finally discharges to the chemisorbed state 1.5 Å above Pt.[71] In the same spirit, Otani et al. performed an ab initio MD simulation, where the charged interface was modeled by Green's function method, and the interfacial potential was established by gradually charging the surface in the course of the simulation.[79] They point out that, upon discharge, the water molecule that releases H^+ to the surface recoils from the surface and reorients to minimize the repulsion between its surface-facing O atom and the negatively charged surface. Therefore, both descreening of H^+ and recoil of H_2O contribute to the overpotential for the Volmer reaction.

The challenge of experimentally capturing the coupled electron and proton dynamics at a solid−liquid interface at comparable atomistic detail has yet to be met by experimental ingenuity. Various spectroscopic and microscopic methods have been developed to probe the molecular identity of the interfacial species, but the potential landscape for charge transfer processes and the fundamental time scales still remain unexplored.[46,80−84] Therefore, we turn to more deliberate surface photochemical and photocatalytic studies where the coupled electron−proton dynamics can be triggered by a photoinduced nonadiabatic change in the interfacial electron distribution, and the response of the light and heavy atoms leading to large displacements of protons or H atoms can in principle be captured in a stroboscopic manner. First we discuss the photochemistry of alkanes on metal surfaces, where the charge transfer-induced dynamics can be deduced, from the scission of C−H bonds and the analysis of the interfacial electronic structure, and next we turn to PCET dynamics of hydrogen bonded methanol overlayers on TiO_2 surfaces.

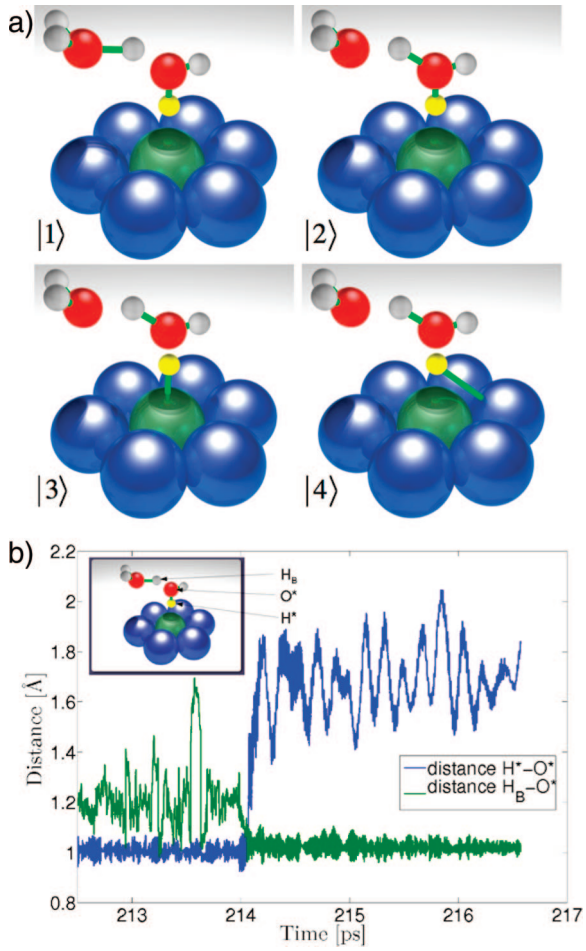

Figure 5. (a) Diabatic states used in an MD simulation for the discharge of H^+ for a Zundel solvated proton cluster on a Pt(111) cluster.[71] The atomic positions in the structures are the same, but the different states represent a proton in the second layer water molecule, |1⟩, a proton localized on the first layer molecule, |2⟩, an H atom on a Pt surface after discharge, |3⟩, and an H atom migrating from the point of discharge, |4⟩. (b) MD trajectory following the motion of a proton within the Zundel cluster in part a at the point of discharge after 214 ps evolution. The discharge is exothermic but requires passage over an energy barrier from the first layer water (O*) to the Pt surface. Reprinted with permission from ref 71. Copyright 2008 American Chemical Society.

3. Photochemical C−H Bond Scission of Chemisorbed Alkanes

The photochemistry of methane on a Pt(111) surface provides an example of electron transfer-mediated proton transfer in the strongly coupled regime. Matsumoto and co-workers studied methane photochemistry at submonolayer to monolayer coverage on a single crystal Pt(111) surface under ultrahigh vacuum conditions.[85−87] At low-temperature (40 K), methane is weakly chemisorbed on Pt(111) in a geometry that has a single C−H bond pointing into the surface.[88,89] Photoexcitation with 6.4 eV light dissociates methane into H and CH_3 fragments, with only a small fraction of CH_3 and CH_4 desorbing from the surface.[86] Similar photochemistry was also found for cyclohexane on a Cu(111) surface, suggesting that photoinduced C−H scission may be common to other alkanes and metal substrates.[90] The mechanism for the surface photochemistry of alkanes on metal surfaces can be rationalized from X-ray absorption (XAS) and X-ray emission spectroscopy (XES) of chemisorbed alkanes; the occupied and unoccupied states of the chemisorbed system and their analysis in terms of the implied charge distributions help to identify the electronic states, the photon induced charge redistribution pathways, and the correlation of electron and proton dynamics that explain the observed photochemistry.[89,91,92]

3.1. Surface Photochemistry of CH_4 on the Pt(111) Surface

Although the weak bonding of methane on the Pt(111) surface suggests physisorption, there is clear spectroscopic evidence for significant molecule−surface electronic interaction. Specifically, vibrational spectra show that the C−H stretching mode, which is triply degenerate in the gas phase, splits into a soft mode belonging to the C−H bond that points into the surface, and weakly perturbed modes of the C−H bonds that point into the vacuum. This perturbation in the vibrational spectrum of methane has been interpreted as evidence for the molecular distortion from the T_d to C_{3v} symmetry through the electronic interaction between the metal facing C−H bond and the metal substrate.[88] The polarization of the molecular charge density away from the surface-pointing hydrogen atom, H_s, to the C atom causes this C−H bond to have substantially lower vibrational frequency than the vacuum facing C−H bonds.[88,93,94] Such softening of C−H_s bonds is a common feature of alkane chemisorption that is believed to be a precursor to C−H bond activation on metal surfaces.[91] Moreover, the bond softening of alkanes on metals also correlates with their activity in C−H bond photodissociation on metal surfaces.[90]

In the studies of surface photochemistry of methane and cyclohexane on metal surfaces, Matsumoto and co-workers found that C−H bond dissociation requires a photon energy of at least 6.4 eV. It is generally believed that surface photochemistry occurs either by a substrate mediated mechanism, where electrons are excited from substrate to an unoccupied state of adsorbate, which is referred to as the hot electron mechanism, or by direct excitation between the occupied and unoccupied states of adsorbate.[95−98] Because there are very few mechanistic studies of surface photochemistry where the excitation of unoccupied states and the ensuing chemistry have been directly observed and correlated, discussions of the excitation/reaction mechanisms usually focus on indirect measurements.[19,29,99] In the case of the CH_4/Pt(111) photochemical system, Matsumoto and co-workers employed the analysis of photoinduced reaction yield on the laser polarization to prove that excitation of methane and cyclohexane occurs through the adsorbate-localized processes.[85,87,90]

The photochemistry of methane in the gas phase can be initiated by excitation of the Rydberg states, which are coupled to the dissociative σ^* states.[87] The photodissociation of alkanes with 6.4 eV light on metal surfaces, which is well below their gas phase HOMO−LUMO gaps of about 10 eV, indicates that the surface plays an essential role. Recall, however, that the image charge interaction reduces the HOMO−LUMO gap of adsorbates interacting with metal surfaces, making it conceivable that the intramolecular transition could be excited when methane is chemisorbed at a metal surface. The chemisorption induced electronic structure and band alignment of the methane-localized states provide further insights into the surface photochemistry of alkanes.

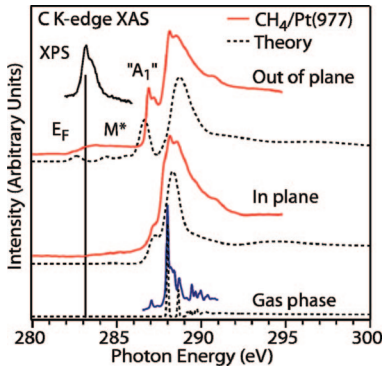

Figure 6. Experimental XAS spectra of CH_4 on a Pt(977) surface (approximately 10% step density) and in the gas phase for the in-plane and out-of-plane directions of the electric field vector of X-ray excitation light shown as solid lines. The dashed lines show the corresponding calculated XAS spectra from DFT calculation. The vertical line denotes E_F determined from X-ray photoelectron spectroscopy (XPS).[89] Reprinted with permission from ref 89. Copyright 2006 American Physical Society.

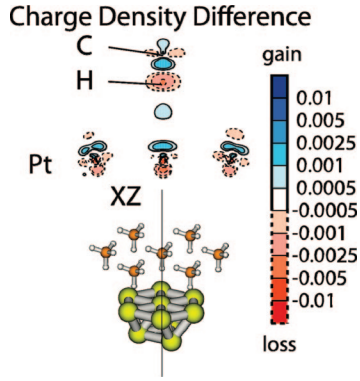

Figure 7. CH_4−Pt-cluster for seven methane molecules chemisorbed on the Pt(111) face, for which the DFT electronic structure calculations have been performed. The charge density difference plot shows a loss of density on the H_s atom and a corresponding gain between the H_s atom and the C atom of methane, as well as the Pt surface.[89] Reprinted with permission from ref 89. Copyright 2006 American Physical Society.

3.2. Surface Electronic Structure of CH_4 on the Pt(111) Surface

Electronic spectra of monolayer thick methane films on platinum surfaces provide detailed evidence for significant electronic interaction between alkanes and metals.[100] The bonding of methane on the Pt(111) surface, and more generally, the interfacial occupied and unoccupied electronic structure, has been examined by XES and XAS spectroscopy.[89,92] The modeling of experimental XAS and XES spectra in Figure 6 by DFT calculations provides a detailed description of the chemisorption-induced interfacial charge redistribution. The calculations were performed for methane adsorbed on the CH_4−Pt-cluster depicted in Figure 7. The spectra are consistent with distorted methane molecules bonding to the surface through the C−H_s bond at a Pt−C distance of 4.15 Å. According to Öström et al., the broad DOS labeled as M in XES spectra that extends from the highest molecule-localized occupied state at ∼4−5 eV below E_F, all the way to E_F (Figure 6a), corresponds to electron density polarized from H_s toward the C side of the C−H_s bond. The calculated chemisorption induced charge redistribution that is responsible for the M feature is shown in Figure 6a. The polarization of charge has been attributed to the Pauli repulsion between the surface and molecule charge densities,[92] but in addition, it is very likely that the image charge repulsion, which has been described in section 2, also makes a contribution. The charge redistribution implies mixing of the bonding and antibonding orbitals, causing the C−H_s bond to elongate from its gas phase value of 1.09 Å to 1.18 Å.[92] The polarization of electron density away from the H_s atom contributes to attractive the molecule−surface image charge interaction that counteracts the Pauli repulsion. Similar to methane, other alkanes also experience the chemisorption-induced charge redistribution, giving rise to the bond softening and the M feature in XES spectra.[91]

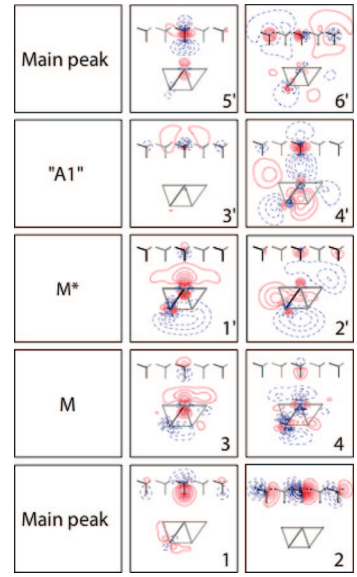

Figure 8. Calculated molecular orbitals (MOs) for the CH_4−Pt-cluster in Figure 7, which are responsible for the XES and XAS peaks identified in Figure 6.[92] Reprinted with permission from ref 92. Copyright 2007 American Institute of Physics.

Öström et al. have also examined the unoccupied DOS of methane covered Pt(111) surfaces by XAS spectroscopy.[89,92] The first sharp feature in the XAS spectra of the CH_4/Pt(111) surface at ∼4 eV above E_F belongs to the $^1A_1$ state of methane, which is predominantly Rydberg in character but also has an admixture of 2s and 2p character.[87,92] Because of its symmetry, the optical transition from the HOMO to the Rydberg state is forbidden by dipole selection rules in an isotropic environment, i.e. the gas phase. The pronounced intensity of this feature in the XAS spectra has been attributed to the aforementioned chemisorption-induced lowering of the molecular symmetry of methane.[89] As indicated in the XAS spectra in Figure 6b, between the Rydberg state and E_F, there is also an extremely broad DOS feature designated as M*, which is also common to larger alkanes. The molecular orbitals corresponding to M* in Figure 8 show it to be mainly of metal character and, therefore, nonbonding with methane.

The XES and XAS spectra identify the possible initial and final states for the surface photochemistry of methane and, in general, alkanes on metals. Chemisorption of methane on metals opens up new excitation channels that do not exist in the gas phase, namely, involving the chemisorption-induced M- and M*-DOS. XAS spectroscopy finds the lowest $^1A_1$ Rydberg state at ∼4 eV above E_F, making it accessible by 6.4 eV excitation from either the adsorbate localized M-DOS below E_F or the high density of d-bands of the Pt substrate. If excitation of the Rydberg state were involved in surface photochemistry as in the gas phase, then the minimum required photon energy would be the energy of the Rydberg

state above E_F. Another possibility, however, is that photoexcitation occurs within methane molecules to the unoccupied M*-DOS from either the highest occupied C−H bonding state, which is calculated to be ∼4−5 eV below E_F,[92] or the adsorption induced M-DOS. The M* ← M excitation is unlikely to have any role in photochemistry, however, because this channel would again proceed with much lower photon energies than 6.4 eV. Although Matsumoto and co-workers initially proposed that photodissociation occurs through the intramolecular excitation of the Rydberg state,[86] following the detailed examination of the electronic structure of chemisorbed methane by Öström et al.,[92] they revised the mechanism to account for the chemisorption induced charge redistribution.[87] Considering the photodissociation photon energy, the most likely scenario for the surface photodissociation of methane on platinum is that it occurs through the promotion of an electron from the HOMO of methane at 4−5 eV below E_F to the M*-DOS;[87] next, we disuss how such excitation could lead to dissociation of the C−H_s bond of methane.

The photodissociation of methane on metal surfaces through the M* ← HOMO excitation is appealing in several respects. To begin with, the C−H bond softening of alkanes suggests that, even in the absence of electronic excitation, the interactions that couple H_s atom motion to the electronic degrees of the surface are already in place. We believe that the C−H bond scission of alkanes corresponds to PCET in the strongly electronically coupled regime. The proposed intramolecular excitation promotes an electron from the HOMO, which is mainly localized on the C−H_s bond, to the M*-DOS, which is localized in front of the metal surface, as shown in Figures 6 and 8. The broad spectral width in XAS spectra probably has contributions from several orbitals that contribute to the M*-DOS. The complete lack of spectral resolution of the M*-DOS, however, suggests that the lifetime of electrons excited to these orbitals could potentially be in the subfemtosecond range. Although deducing lifetimes from surface electronic resonance line widths should be done with caution,[21] the most facile interpretation in this case is that the line widths represent the delocalization of electrons from M* into the isoenergetic bulk bands of the substrate on a time scale that is significantly faster than even H atom motion.[101] Therefore, by photoexcitation, an electron is transferred from the C−H_s bond to the substrate, leaving a photohole, which weakens the C−H_s bond and reduces the electron density on the H_s atom further. The situation generated by photoexcitation is similar to the Volmer reaction, except that the positive charge excited within a methane molecule cannot be screened by molecular solvation within the methane overlayer. By weakening the C−H_s bond, the hole, i.e. proton, is attracted more strongly by its image charge, which draws it into the metal surface, severing the C−H_s bond. Developing the methods that can follow the attosecond time scale correlated electron−proton dynamics following photohole generation in alkanes and similar surface photochemical processes is a challenge for both experiment and theory.[20,102]

Photodissociation of the C−H_s bond in methane occurs in competition with the recombination of the photohole with electrons in the Fermi sea of the substrate. If the hole quenching can compete with the bond dissociation, then the reaction quantum yield should depend on the speed of the proton transfer and, therefore, show a deuterium isotope effect. Indeed, Matsumoto and co-workers report that the cross sections for methane photodissociation decrease from 1.8×10^{-19} to 1.3×10^{-19} cm^2 between CH_4 and CD_4,[103] which corresponds to precisely the reduced mass factor of $\sqrt{m_D/m_H} = 1.4$ expected for the relative speed for H vs D atoms. The observed isotope effect, therefore, is consistent with the competition between H^+ transfer from chemisorbed CH_4 to the Pt(111) surface and Auger decay of the photohole excited on a CH_4 molecule.

To conclude this discussion, both the chemisorption properties and the photochemistry of methane indicate strong coupling of electron and proton motions at a Pt surface. As in the example of the Volmer reaction, H^+ is transferred between adsorbate and substrate under the influence of its image charge. In the electrochemical case, a proton is solvated by H_2O molecules, so the proton transfer is controlled by solvation dynamics. In the photochemical case, light-initiated electron transfer generates a nearly bare proton at the nucear configuration of heavy atoms of the ground state; the deuterium isotope effect suggests that the discharge is governed by unbounded H atom motion on a surface defined by the heavy atoms. The light-induced H^+ discharge offers the possibility to follow the surface attochemistry of the correlated electron and proton dynamics. Similar ultrafast correlated electron−proton dynamics upon core hole excitation of O atoms in liquid water have been gleaned through simulations of the oxygen K-edge of XES spectra.[104]

3.3. H_2O Interaction with Metal Surfaces

One might ask whether similar chemisorption-induced electronic interactions as observed for CH_4 on Pt(111) could also occur for other adsorbates, such as H_2O or NH_3, on metal surfaces. Although detailed surface photochemical studies that identify the electronic states are not available, in the past few years significant effort has been made to understand the interaction of water with metals from both the experimental and theoretical perspectives.[105−107] The bonding of water to metal surfaces can occur through metal−H_s atom hydrogen bonds and/or through lone pair electron interactions on O atoms and the metal surface. These interactions can be stronger, weaker, or comparable to the intermolecular hydrogen bonding in water. In forming metal−H_s hydrogen bonds, the charge density increases on the metal side of the H atom and decreases on the O atom side.[108−111] Unlike methane, however, the cooperative interactions between molecules are quite strong, as already discussed in the case of the Volmer reaction. Recent femtosecond laser studies of water overlayers on metals suggest that the dynamics induced by 1.5 eV photons are dominated by the energy transfer from hot electrons to the water overlayer, which mainly induces molecular diffusion, rather than photochemistry.[112,113] XES spectra, however, show a resonance at 5 eV below E_F, which has predominant O−H bonding character and is similar to the HOMO of methane. By analogy to methane, it may also be possible to generate localized hole states in different O−H bonds, e.g. those forming a hydrogen bond with the metal or those between water molecules, and thereby initiate proton transfer processes between molecules and the surface or within the H_2O overlayer. By inducing and monitoring such photohole induced dynamics in an H_2O overlayer, one might be able to follow the Volmer reaction dynamics with the moelcular environment specificity and ultrafast time resolution.

4. PCET in Methanol Covered TiO_2 Surfaces

Next we explore the nature of electron acceptor states on protic-solvent covered metal oxide surfaces. Metal oxide surfaces under atmospheric conditions are covered by an overlayer of water and surface bound OH species.[24,114,115] Photoexcitation by visible or UV light can transfer electrons from a metal oxide substrate to such an overlayer and, thereby, induce chemical transformation of the overlayer or chemistry with coadsorbed molecules.[23] By means of 2PP spectroscopy, we investigated the electronic structure and electron induced solvation dynamics for H_2O and CH_3OH covered TiO_2(110) surfaces.[23,116−118] These experiments identified the lowest energy vertical electron acceptor states in protic solvents, namely the partially solvated or "wet electron" states. Photoinduced CT transfers electrons from the semiconductor substrate to the most electropositive sites in the protic solvent overlayer. These electropositive sites are mainly the dangling H atoms, which are not able to form strong hydrogen bonds (HBs). Wet electron states correspond to electrons partially solvated on several H atom centers that can be distributed over different adsorbate molecules or surface OH species. The wet electron state populated by vertical excitation does not correspond to the most stable wet electron structure. Therefore, the following excitation electrons can be energetically stabilized through solvation involving both the substrate and adsorbate structural rearrangement. Because H atoms are the acceptor sites, PCET may be a particularly efficient mechanism for stabilizing the excess charge. The inertial and diffusive solvation by the interface occurs in competition with the wet electron decay by reverse charge transfer (RCT) to the resonant conduction band continuum of the substrate.

We will first describe the wet electron states for H_2O overlayers on TiO_2 surfaces, because they are likely to be the dominant electron acceptor states in many important interfacial phenomena at metal oxide−aqueous interfaces.[23] Next, we will discuss methanol covered TiO_2 surfaces, where we found electron dynamics (population and energy relaxation) to be strongly influenced by deuterium isotope substitution. We interpreted the isotope effect based on wet electron electronic structure calculations as evidence for electron decay into the conduction band of TiO_2 by a PCET mechanism.[118]

4.1. Wet Electron States on Reduced H_2O/TiO_2 Surfaces

4.1.1. Occupied and Unoccupied Electronic Structure of H_2O/TiO_2 Surfaces

We discovered wet electron states in 2PP spectroscopic measurements on bare and H_2O molecule covered single crystal TiO_2(110) surfaces. 2PP spectra were excited with 400 nm (3.1 eV photon energy) excitation light, delivered in 10 fs duration pulses.[119] The excitation photon energy is sufficient to excite across the 3.0 eV indirect band gap of TiO_2,[120] but electrons near the conduction band minimum (CBM) cannot be detected by absorption of another 3.1 eV photon, because the work function of TiO_2, which ranges from ∼5.6 eV for a stoichiometric TiO_2(110) surface to ∼3.5 eV for H_2O or CH_3OH covered surfaces,[119] is higher than the photon energy. Therefore, 2PP excitation can only be initiated from initial states belonging to the occupied Ti-3d defect band of reduced TiO_2 surfaces, which extends from E_F to the maximum DOS, ∼0.9 eV below E_F, in conventional photoemission spectra.[121] The excitation photon energy is sufficient to induce 2PP from these defect states and to probe the electronic structure and dynamics of unoccupied states, typically between 0.5 and 3.0 eV above the CBM.

Ti-3d defect states can be created by various procedures for reducing TiO_2 surfaces. TiO_2 can be reduced by introducing surface and bulk O atom vacancies (O_v) with density and spatial distributions that can be controlled by thermal (annealing in vacuum or in O_2 atmosphere) and nonthermal (e.g., electron irradiation) surface preparation techniques.[119] Oxygen atom vacancies are readily generated on the bridging oxygen (O_b) rows, which run in the [001] crystallographic direction above the surface plane. Removing a single O atom from the TiO_2(110) surface transfers a pair of electrons to the Ti-3d defect band.[121] The spatial distribution of the surface Ti-3d density of single O_v defects has been characterized by low temperature STM: at 77 K the density is distributed symmetrically over multiple five coordinate Ti_{5c} sites along the [001] crystallographic direction,[122] whereas, at 4 K, the density is more localized in an asymmetric distribution attributed to polaron formation.[123] At O_v vacancy sites, molecules such as H_2O and CH_3OH dissociate without an apparent barrier to form either two OH species or OH and CH_3O species, which are incorporated through their O atoms into O_b rows.[124−128] The H atom or CH_3 groups on top of O_b rows also have the reducing capacity, as they transfer a single electron to the Ti-3d defect DOS.[122]

The experimental 2PP spectra of H_2O/TiO_2(110) surfaces show strong differences in the unoccupied state DOS depending on whether the initial TiO_2 surface is stoichiometric or has been reduced before H_2O dosing.[116] 2PP spectra of the stoichiometric TiO_2 surface were featureless for H_2O coverages up to several MLs, as can be seen in Figure 2 of ref 116, whereas reduced surfaces had a strong resonance 2.3 eV above E_F that achieved maximum intensity for ∼1 ML of H_2O coverage.[116] The resonance could be reproduced by various reducing preparations of the TiO_2 surface, such as thermal annealing, electron bombardment, and H atom irradiation.[23,116] Independent of the mode of preparation, reduced surfaces were covered by a fraction of a monolayer of bridging OH species after exposure to H_2O. Thus, to observe the 2.3 eV resonance in 2PP spectra requires both 1 ML of H_2O and a fraction of a monolayer of bridging OH to be present on TiO_2 surfaces.

In order to assign 2PP spectra, we performed plane-wave DFT calculations on the unoccupied states of OH and H_2O covered TiO_2 surfaces for different adsorbate coverages, adsorption structures, and degrees of surface reduction.[129] Based on the experimental observations that the resonance appears only on reduced surfaces where surface OH is present and its intensity depends on the H_2O coverage, and theoretical calculations, which identified electron acceptor states for various OH and H_2O structures on TiO_2, we concluded that the 2.3 eV resonance is due to molecular overlayer structures where the unoccupied orbital is distributed over several H atom sites, such as shown in Figure 9.[116] In the DFT calculations, the largest density of the unoccupied orbital on reduced surfaces is always associated with the dangling OH species, which can interact with neighboring water molecules only through very weak HBs. For the typical wet electron orbital in Figure 9, the unoccupied density spreads from the primary OH acceptor site to several secondary sites on H atoms of a neighboring H_2O molecule

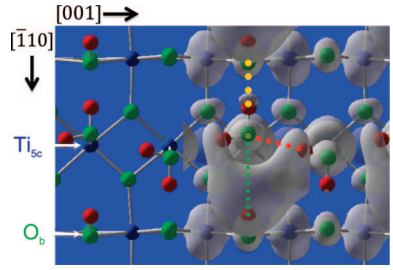

Figure 9. Calculated chemisorption structure and wet electron orbitals (gray orbs) of 1 ML of H_2O and 0.5 ML of H (forming bridging OH), on a rutile TiO_2(110) surface. Blue, green, and red spheres indicate, respectively, Ti, O, and H atoms. The green, red, and yellow dotted lines connect H and O atoms involved in progressively stronger hydrogen bonds, correlating progressively reduced wet electron orbital density.[116,129]

that are also involved in weak intermolecular HBs.[130] For this and similar structures, wet electron state energy is calculated to be 2.6 eV above the CBM, which is close to the experimental value of 2.3 eV. The spatial extent over which wet electron orbitals can delocalize over multiple acceptor sites determines the degree of their stabilization.[129] In addition to the H atom acceptor sites, it should be recognized that the image charge interaction also contributes to the experimental wet electron orbital stabilization but is not included in DFT calculations.[27] Because of the role of surface OH, the strong effect of the metal oxide surface on the H_2O molecule chemisorption structure, and the image charge interaction, wet electron states have intrinsically interfacial character.

4.1.2. Nature of Acceptor States on H_2O/TiO_2 Surfaces

On the stoichiometric TiO_2 surfaces, only H atoms on H_2O molecules can act as the acceptor sites. Because these sites are less acidic (electropositive), they do not stabilize wet electron states as efficiently as surface OH, and therefore, the wet electron resonances for stoichiometric surfaces are too high in energy to excite with 3.1 eV photons.[129] The electronic states of thick water overlayers, such as the conduction band and the partially solvated surface states of the water−vacuum interface, which have been studied by Wolf and co-workers,[14,35,36,131] are expected to be at a higher energy than the wet electron states on reduced TiO_2 surfaces.

We also investigated the population and energy decay dynamics of wet electron resonance on a H_2O/TiO_2 surface by TR-2PP. The lifetime of wet electron resonance saturates for 1 ML of H_2O coverage at 15 fs, and the energy of the resonance does not appreciably change on this time scale. The resonance decay probably occurs through RCT to the conduction band of TiO_2. The photoemission cross section appears to be far lower for hot electrons in the conduction band of TiO_2 than for wet electron surface states; therefore, even though the donor and acceptor states might be at the same energy, the experiment is sensitive mainly to the decay of the surface wet electron population by RCT. The time scale for RCT is on the order of the period of the O−H stretching vibration and, therefore, is insufficient for the H_2O overlayer to undergo structural reorganization that would stabilize wet electrons through solvation. Although the O−H stretching vibration might help to stabilize wet electrons, slower modes involved in breaking the existing HBs to generate dangling H atom acceptor sites, such as reorientation or bending of O−H bonds, are likely to be more effective in stabilizing wet electron states.[132] Significantly, TR-2PP measurements on D_2O covered surfaces gave essentially the same wet electron resonance lifetime, indicating that the RCT process may not be sensitive to a solvation induced molecular response. It is also possible that isotope effects on the nonadiabatic couplings and Franck−Condon overlaps counteract each other to give no net isotope effect, as is known to happen in the nonadiabatic relaxation rate of the hydrated electron.[133]

The RCT dynamics measured in the experiment of Onda et al. have been simulated by Fischer et al. using the *ab initio* nonadiabatic molecular dynamics method for OH and H_2O covered TiO_2 surfaces.[132,134] They found that both nonadiabatic and adiabatic processes contribute to RCT on the ~10 fs time scale, which is comparable, though somewhat faster, than the experimentally measured value. The adiabatic contribution is significant even though RCT is promoted by modes with vibrational periods that are much longer that the observed 15 fs lifetime,[116] because, within a fraction of a vibrational period, the coupling modes induce many crossings between the donor and acceptor states. Even though they have less orbital density, vibration of H_2O molecules is more effective in promoting RCT than the OH species because the former modulates both the wet electron state energy and the coupling to the TiO_2 surface, whereas the latter only affects the energy. The RCT is particularly efficient because, according to the DFT calculations, the wet electron orbital density is nearly 50% within the TiO_2 substrate.[129,134] The relaxation pathway identified by Fischer et al. involves charge transfer from wet electron states to a surface state of TiO_2, followed by transfer to TiO_2 bulk states. The theoretical RCT time scale might be somewhat faster than the experimental one, because DFT calculations do not include the image potential, and therefore, the bulk contribution to wet electron states is overemphasized. Prezhdo and co-workers found similar RCT dynamics for dye-sensitized charge injection from organic molecules to the conduction band to TiO_2.[132,135,136]

4.2. PCET in CH_3OH/TiO_2 Surfaces

4.2.1. Overview of Experiments on CH_3OH/TiO_2 Surfaces

In an extension of experiments on wet electron states of H_2O/TiO_2 surfaces, we investigated related phenomena for CH_3OH/TiO_2 surfaces.[117,118,137] As in the case of H_2O adsorption, continuous dosing of a TiO_2 surface at a surface temperature of 100 K with CH_3OH leads to the appearance of a new resonance in 2PP spectra that shifts from ~2.6 eV with respect to E_F at submonolayer to ~2.0 eV at multilayer CH_3OH coverage. By annealing the multilayer sample at different temperatures, we established that, just as in the case of H_2O, the resonance attains the maximum intensity at 1 ML of coverage at 2.3 eV.[117,118] Based on its interfacial nature and electronic structure calculations for methanol overlayers on a TiO_2(110) surface, we established that the methanol resonance has a similar origin to the wet electron state on H_2O/TiO_2 surfaces.[116] In contrast to the H_2O-TiO_2 interface, however, the dangling H atoms on a CH_3OH/TiO_2 surface are available only on the CH_3 group of methanol. The OH groups participate in strong intermolecular and molecule−surface HBs, which make them poor acceptor sites for wet electrons.[137] Therefore, even though in free methanol molecules H atoms on CH_3 groups are less acidic than the OH, on surfaces they may become more acidic through charge transfer to the substrate. Moreover, they present multiple proximate dangling centers, which can stabilize the wet

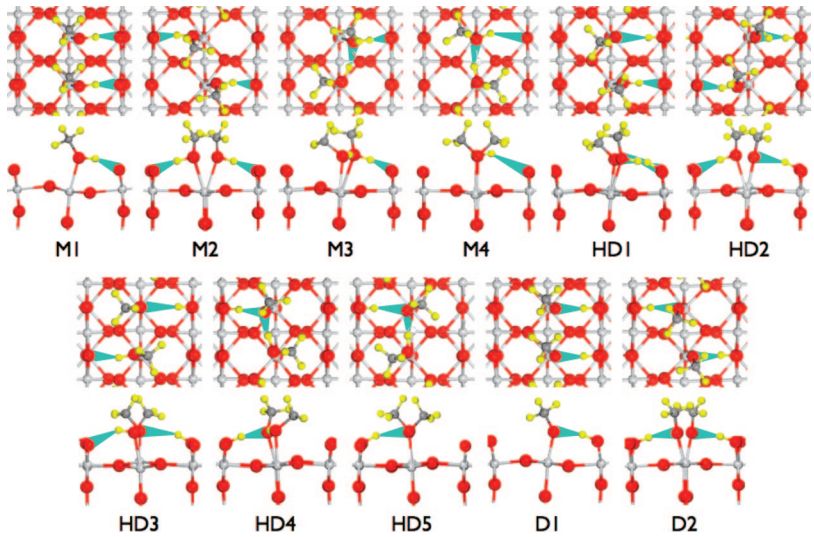

Figure 10. Calculated top and side views of chemisorption structures for two methanol molecules per (2 × 1) TiO_2(110) surface unit cell. Light gray, red, dark gray, and yellow spheres indicate respectively Ti, O, C, and H atoms. Blue rays connect H and O atoms participating in HBs. M, HD, and D designate molecular, singly deprotonated, and doubly deprotonated methanol structures.[137]

electron resonance on the CH_3OH/TiO_2 surface. Excitation of the wet electron resonance through a photoinduced charge transfer process initiates complex dynamical evolution of the excited state involving both the nonexponential population decay and stabilization of the excited state energy relative to the Fermi level; based on an observed deuterium isotope effect, we attributed these complex dynamical processes, in part, to ultrafast interfacial PCET.[118] Because the original discovery of PCET on CH_3OH/TiO_2 has been reviewed,[23] we briefly recall the original experimental observations and their interpretation, and we discuss the PCET dynamics in light of the recent theoretical simulations of ET and PCET on protic solvent covered semiconductor surfaces.[134,138]

4.2.2. Chemisorption Structure of CH_3OH/TiO_2 Surfaces

First we will describe the chemisorption structure of methanol on TiO_2 based on DFT calculations, and subsequently, we will present the experimental and theoretical justification for the calculated structures. Recently we performed extensive calculations on methanol chemisorption structures and the corresponding wet electron states.[137] We reported a total of 11 chemisorption structures for two methanol molecules per (2 × 1) TiO_2 unit cell where either or both molecules can be in the molecular form, singly deprotonated, or doubly deprotonated, as shown in Figure 10.[137] Methanol molecules bind to Ti_{5c} sties through their O atoms, while the OH forms either intermolecular or molecule−surface HBs.[137,139,140] The structures were obtained for different combinations of molecule−surface or molecule−molecule HBs. The deprotonated form corresponds to transfer of an H atom from the OH of methanol to the closest O_b atom of the surface. The calculated chemisorption energies range from 0.63 eV for the most stable molecular structure (M3 in Figure 10) to 0.30 eV for the least stable doubly deprotonated one (D1). In general, molecular chemisorption structures are the most favorable ones and single and double deprotonation to form methoxy at Ti_{5c} sites and bridging OH leads to progressively less stable structures. Deprotonation raises the energy of the O-2p derived HOMO level, but this is just one factor that contributes to the overall trend in the total energy. Also, intermolecular HBs seem to provide stronger binding than molecule−surface ones, but structures with only intermolecular HBs are unstable with respect to those forming alternating molecule−molecule and molecule−surface HBs because of steric hindrance between the methyl groups within the (2 × 1) unit cell. Also, chemisorption causes surface stress, which is probably caused both by molecules tilting to form HBs and by charge transfer to the substrate.[137] It is likely that many of the calculated structures would be present in a methanol monolayer formed by low temperature deposition from the gas phase. The barriers for interconversion between structures are not known but would reflect the activation energies for breaking HBs and for proton transfer between adsorbate and substrate. We note that calculations for at least 11 layer thick slabs are required to obtain converged chemisorption energies.[137] This indicates that calculations performed on TiO_2 clusters are likely to suffer from finite size effects in terms of energies for both the chemisorption as well as the band gap of TiO_2.[120,141]

Based on UHV temperature programmed desorption (TPD) studies on stoichiometric single crystal TiO_2(110) surfaces, Henderson et al. proposed that methanol can chemisorb in both the molecular and deprotonated forms.[139] Suggestive evidence for the partial dissociation is that, unlike water, which has a single monolayer desorption peak, methanol TPD spectra show two peaks at 295 and 350 K that have been assigned respectively to desorption of CH_3OH from the molecularly chemisorbed form and through the recombinative desorption of H and methoxy fragments.[139] In submonolayer coverage STM measurements at 300 K, Zheng et al. found methanol dissociation only at O_b vacancy defect sites to form bridging OH and CH_3O species but not at Ti_{5c} sites of the stoichiometric surface.[125,128] They also found that methanol molecules catalyze OH migration from one O_b row to another, which can happen by a concerted process when a methanol molecule forms a double HB—one between the bridging OH of the surface and the O atom of methanol and the other between the OH of methanol and the O_b atom of the adjacent bridging row. For this double HB structure, proton transduction can occur in a concerted manner as in a Grotthuss-like proton conduction.[77] This suggests that intermolecular interactions between chemisorbed methanol molecules or their dissociation fragments on O_b rows can promote thermal methanol deprotonation.

4.2.3. Hole-Mediated Processes on CH_3OH/TiO_2 Surfaces

Methanol is known to be a hole trap on TiO_2 surfaces.[142] EPR measurements on hydroxylated TiO_2 colloids indicate that methanol radical and CH_2OH form through an outer sphere hole transfer process.[143,144] Chemisorbed methoxy on TiO_2 colloids also forms methanol radical, but it decomposes further through a multiple photon process into other decomposition products.[143] Methanol deprotonation can also be a photocatalyzed process. Our DFT calculations show that the methanol/methoxy O-2p valence states are at −0.5/−0.4 eV below the valence band maximum (VBM) of TiO_2 when averaged over the different molecular and singly deprotonated structures in Figure 10.[137] Considering the error in the DFT band gap of TiO_2,[120] these adsorbate-localized states might even be above the VBM. Therefore, VBM holes generated by band gap excitation can localize on O atoms of chemisorbed CH_3OH. If a hole were to be captured by a chemisorbed methanol molecule, and if the molecule were engaged in an HB to the proximate O_b atom, then the transfer of an H atom across the HB would lower the hole energy on the thus formed methoxy. Therefore, the hole stabilization would favor deprotonation of methanol to form methoxy. Even though the deprotonated form is less stable, the hole stabilization energy approximately compensates the difference between the total energies of molecular and deprotonated structures, suggesting that hole capture by methanol could result in photocatalytic deprotonation of methanol.[137]

In order to explore this possibility further, in Figure 11 we plot the charge difference between the M3 and HD4 structures in Figure 10, which are related by proton transfer through a molecule−surface HB. Although the charge densities in Figure 11 are the static ones for the initial and final states that could be interconverted by hole transfer, they do capture the charge redistribution associated with proton transfer across the HB. Specifically, deprotonation takes charge from the H atoms of the CH_3 group and the O−H bond of methanol and transfers it to the O−H bond of the bridging row and the Ti−O and O−C bonds of methoxy. Minor charge redistribution also occurs in the charge density of the O−H bond of the neighboring methanol molecule. Clearly, the photocatalytic deprotonation of methanol is an interesting, yet hardly explored, case of an inner sphere PCET process, which may play a role in a photocatalytic oxidation of alcohols. We note that recently Du et al. proposed a theoretical model for the photocatalytic oxidation of polyhydroxyl molecules on TiO_2, where they discuss hole-mediated deprotonation processes.[145]

The various calculated chemisorption structures that have been identified in Figure 10 define the vertical wet electron acceptor states, which could be contributing to the experimental 2PP spectra and PCET dynamics. The calculated acceptor orbitals in Figure 7 of ref 137 are all dominantly distributed over several dangling H atoms of the CH_3 groups of methanol and methoxy. There is essentially *no* density on OH species on methanol or bridging O atom rows. The calculated wet electron state energies span the 2.40−3.26 eV range for the various structures, with a clear correlation with the surface dipole density.[137] This is not surprising, because the surface dipole potential, in addition to the image potential, which is not included in the calculation, will stabilize excess electron states at a solid−vacuum interface. There is no apparent correlation, however, between specific structural motifs or binding energies and wet electron binding energies or the dipole densities. Such correlation may be lacking because intermolecular HBs and steric hindrance between methyl groups may affect the binding energies and chemisorption induced charge transfer in structure specific ways.

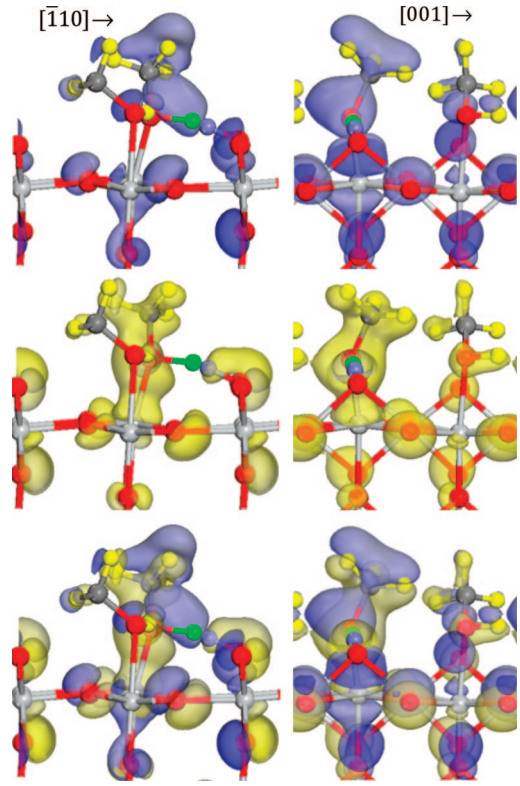

Figure 11. Side views of the M3 and HD4 structures in Figure 10 along the [1̄10] and [001] directions showing the charge difference between the two structures, which is mainly caused by proton transfer within a molecule−surface HB. In the top and middle panels, the blue and yellow orbs show, respectively, the charge surface of the M3 structure relative to HD4 and the same for HD4 relative to M3. The bottom panel shows a composite of the upper panels. Light gray, red, dark gray, and yellow spheres indicate respectively Ti, O, C, and H atoms on methyl groups; the green and blue spheres show the H atom of OH in methanol and on the O_b row, respectively.

The calculated energy range for wet electron states for 1 ML structures of CH_3OH on TiO_2 are in reasonable agreement with experiment. Inclusion of the image potential would bring the electronic structure calculations into better agreement with experiment. We note, however, the reported 2PP measurements are for reduced surfaces, whereas the calculated results so far have been for stoichiometric TiO_2. To simulate the situation for reduced surfaces, we performed additional calculations for the M3 and HD4 structures where we added 0.5 ML of H atoms to O_b rows. This resulted in 0.62 and 1.12 eV reduction of wet electron states for the two structures, respectively. The additional stabilization can be exclusively attributed to the increased dipole density rather than redistribution of wet electron density to the additional bridging OH species. This provides further support that when H atoms are involved in favorable HBs, they make poor wet electron acceptor sites. The role of methyl H atoms as wet electron acceptor sites on TiO_2 surfaces is entirely consistent with conclusions from electron solvation studies in methanol clusters and the liquid phase.[146−150]

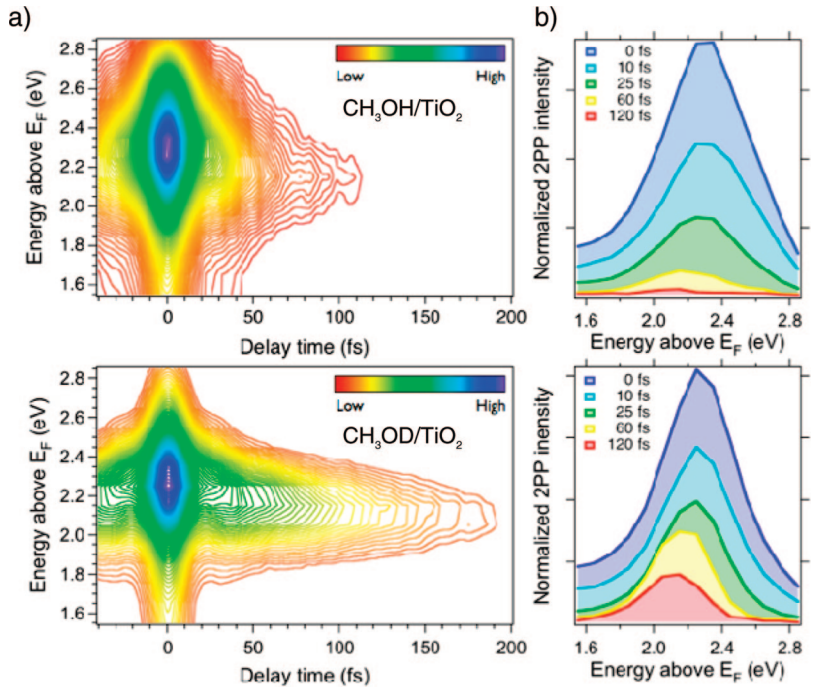

Figure 12. (a) Pump−probe time-resolved two-photon photoemission measurements at 14 different energies combined into contour plots to show the intermediate wet electron state population dynamics in the 2PP process for CH_3OH/TiO_2 (top) and CH_3OD/TiO_2 (bottom) surfaces. The molecular coverage in both cases is ∼1.5 ML. (b) Cross sections of pump−probe measurements in part a at several delays showing changes (amplitude and peak energy) in the wet electron resonance for different delay times. The slower population decay for the CH_3OD surface, which is evident in both parts a and b, arises from the D isotope effect on PCET dynamics.[118,151]

4.2.4. PCET Dynamics on CH_3OH/TiO_2 Surfaces

Next we briefly discuss the experimental results on wet electron state dynamics. Figure 12 shows the experimental 2PP spectra for ∼1 ML of CH_3OH and CH_3OD on a reduced TiO_2(110) surface and a plot of wet electron population decay derived from the time domain measurements for 14 different energies near the wet electron resonance.[151] The spectra show that, for approximately the same molecular coverage (1.5 ML in Figure 12), the CH_3OD wet electron state peak is more intense and the population decay dynamics extend to a longer time scale. Both the spectra and the lifetimes depend on the coverage, as discussed previously.[118] Here we confine our discussion to conditions where single monolayer coverage conditions prevail.

As described previously, the wet electron state decay is composed of a fast (∼30 fs), an isotope independent, and a slow coverage, and isotope dependent processes. Vertical excitation promotes electrons from the Ti-3d defect band to wet electron orbitals such as shown in Figure 13 for the HD4 structure. The excited state population decays initially through a fast, isotope independent process, which we believe involves RCT of electrons into the resonant states of the conduction band of TiO_2. This channel is turned off through the ballistic nuclear response involving one or more coordinates. The photoexcitation creates a force initiating wave packet motion on the excited potential surface toward a nuclear configuration that can stabilize the redistributed charge. The decay from or near the vertically excited state can be rapid because of favorable Franck−Condon overlap with the ground state. The nuclear response most likely involves the stiffening of Ti−O bonds in response to creation of a hole in Ti-3d defect DOS, i.e. screening of the photohole, and probably fast modes of the acceptor states, such as the C−H stretching vibrations. The primary wave packet motion brings the excited state to a nuclear configuration where the coupling to the substrate is weaker. The subsequent decay exhibits a deuterium isotope effect of ∼2, indicating that further decay is strongly coupled to proton or H atom motion. In ref 118 we described a scenario for the HD1 structure in Figure 10 where wet electron is stabilized primarily by the dissociation of the bridging OH-methoxy HB and secondarily by proton transfer from a methanol molecule to an O_b atom through a molecule−surface HB. Here, in Figure 13, we present results of a Δ-SCF calculation for the HD4 structure, which exhibits some important similarities and differences with respect to the HD1 structure.

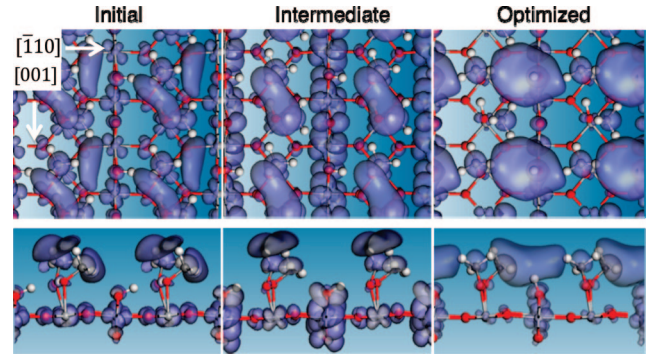

Figure 13. Top and side views of wet electron orbital distributions for the HD4 structure at different stages during Δ-SCF excited state optimization. At the start of the optimization, electron is added to the wet electron orbital (translucent orb) in the ground state molecular geometry. During the optimization, the charge density flows initially from orbitals mainly localized on H atoms of CH_3 groups, to the O_b row. An increase in charge density near OH on the O_b row causes OH to break its hydrogen bond to the O atom of methoxy and rotate to a nearly vertical configuration, where it stabilizes wet electron on top of a surface OH in a pocket formed by neighboring methanol and methoxy CH_3 groups.

Δ-SCF is theoretical method for calculating excited state diabatic potential energy surfaces starting from a ground state

electronic structure calculation.[152,153] It is a density functional method resembling a standard DFT calculation except that one or more electrons or holes are placed in normally unoccupied Kohn−Sham orbitals before minimizing the energy of the system. We performed Δ-SCF calculations for various structures in Figure 10 by using the geometry of the ground state from the DFT slab calculation as the starting point. Wet electron states were identified as described in ref 129, and an electron was placed into the lowest energy wet electron orbital. The optimization was performed for the molecular overlayer corresponding to 1 ML of coverage and a 1 layer thick TiO_2 substrate. The substrate had to be kept at the minimum thickness to reduce the likelihood of the excited state electron decaying into its conduction band in the course of energy minimization. Despite this precaution, for many structures the calculations terminate with the irreversible decay of wet electron into the substrate. For the calculations where electron survives within the molecular overlayer, Δ-SCF calculation provides valuable information on the structural rearrangements that stabilize wet electrons within the molecular overlayer.

Figure 13 shows the top and side views of the initial, intermediate, and final wet electron orbital distributions during Δ-SCF optimization of the HD4 structure. The initial distribution has the wet electron state spread over two lobes covering several dangling H atoms of the CH_3 groups of methanol and methoxy forms within the unit cell. In the intermediate structure, the lower wet electron lobe of the overlayer vanishes, while the upper lobe grows; moreover, charge density appears within Ti−O bonds of the bridging O row. At this stage, the molecule−surface and intermolecule HBs remain intact and the wet electron orbital density is absent from the OH of methanol and on O_b rows. In the final optimized structure, the HB between methoxy and the OH on the O_b row have broken, allowing the newly dangling H atom of OH to interact with the wet electron. The wet electron orbital is confined within a pocket formed by bridging OH, which is now the primary solvation site, and dangling H atoms of four neighboring methanol and methoxy groups, which are the secondary solvation sites. In addition to the large amplitude reorientation of the bridging OH, breaking of the HB allows the methoxy group to assume a more upright position. We attribute the primary origin of the D isotope effect to breaking of the HB between bridging OH and its neighboring methoxy or methanol molecule at Ti_{5c} sites; the same process was also found in Δ-SCF calculations for the HD1 structure.[118] The vertical excitation injects electrons into wet electron orbitals that are localized on H atoms of CH_3 groups and that can be decoupled from RCT by the initial wave packet motion. On a longer time scale, dissociation of the bridging OH hydrogen bonds to form dangling surface H atoms stabilizes the wet electron state energy, thereby minimizing the energy of the entire surface by 0.42 eV for the HD4 structure and bringing wet electrons in closer contact with the TiO_2 surface. As seen in the case of the H_2O/TiO_2 system, the bridging OH sites are the minimum energy electron acceptor states on protic solvent covered TiO_2 surfaces, which mediate RCT on the 15 fs time scale. Therefore, the bending motion of bridging OH from the initial HB to the vertical position modulates the wet electron coupling to the substrate and thereby imposes the D isotope effect on the wet electron decay.

Based on the Δ-SCF calculations presented here an in ref 118 as well as theoretical modeling by the Prezhdo[134] and Hammes-Schiffer[138] groups of wet electron and interfacial PCET dynamics, we arrive at the following conclusions. Methanol covered TiO_2 surfaces can stabilize photoinjected electrons either through H atoms of CH_3 groups or surface OH. The OH of methanol appears to be an ineffective acceptor site because it is constrained by its CH_3 group from ever assuming near a vertical position, where it could interact strongly with wet electrons; for the H atom of the methanol OH to interact with a wet electron orbital, it first must transfer to the O_b row and then assume a vertical configuration, as we described for the HD1 structure in ref 118. The initial acceptor sites on CH_3 groups of methanol and methoxy can probably respond to the excess charge through C−H bond stretching or CH_3 group rotation, but Δ-SCF calculations do not indicate significant forces that would excite these motions. The excited state potential energy is most effectively reduced by breaking the surface-to-molecule HB to allow surface OH to point up, where it can interact most effectively with the wet electron density. The correlated bending of surface OH into the vertical configuration and descent of wet electron density from CH_3 groups to OH, either through space, as shown in ref 118, or via the substrate, as in Figure 13, is responsible for the D isotope effect observed in CH_3OH/TiO_2 surfaces. Although methanol covered TiO_2 surfaces could be highly inhomogeneous, as suggested by Figure 10, Δ-SCF calculations for different initial structures find the common structural motif for stabilizing wet electron states to be the formation of dangling surface OH. Although the Δ-SCF method is a crude approach, it provides valuable insights into the excited state electronic structure and molecular dynamics of the photocatalytic PCET process, for which, at present, there is no alternative slab or cluster based theoretical approach.

5. Summary and Conclusions

In this review we have described recent experimental and theoretical research on ultrafast interfacial inner sphere PCET dynamics. What makes interfacial PCET processes unique is the presence of a strong potential gradient that imposes opposing forces on electrons and protons within a spatial region that is, at most, a few angstroms wide. Because of the strong but tunable gradients, whether a PCET process occurs through separate proton and electron transfer steps or through a concerted process can have a significant impact on the activation energies and overpotentials that are required for a chemical reaction. Considering that tantalizing photocatalytic processes, such as the decomposition of H_2O into H_2 and O_2 and the reduction of CO_2 into chemical fuels,[11,154,155] have been demonstrated with band gap excitation of TiO_2 surfaces, it is highly desirable to explore the reaction mechanisms and to devise chemical pathways that perform the multiple electron and proton transfer steps as close to the thermodynamic limit as possible. In addition to the complexity of describing chemical processes under strongly inhomogeneous potentials, it is also necessary to devise experimental methods that can probe ultrafast charge transfer processes at interfaces. Techniques such as time-resolved two-photon photoemission provide the means to probe interfacial charge transfer dynamics on time scales that range from a few femtoseconds to longer. The recently developed attosecond laser technology is promising for time resolving even faster processes,[156] as attested by measurements of electron transport through a metal interface.[157] Electron spectroscopic methods, however, are limited to well-defined

surfaces under UHV conditions where photoelectron energy and momentum can be related simply to the properties of the excited states of the system. It is also desirable to develop and employ other methods, such as X-ray scattering and surface nonlinear spectroscopy,[46,158,159] which can provide chemical and dynamical contrast under more realistic chemical reaction conditions.

Ultrafast interfacial PCET also presents substantial challenges for theory. In addition to the difficulty of describing the interfacial potential and, associated with it, the inhomogeneous screening by the fast and slow degrees of freedom of the system, it is also a challenge to treat the electron and proton degrees of freedom on an equal basis, as described elsewhere in this Special Issue.[4] This is the case for PCET processes occurring under near equilibrium conditions, but challenges are particularly severe for excited state processes, such as would predominate under photocatalytic conditions. Nevertheless, several groups are paving the way to develop methods that are starting to provide valuable insights and powerful tools for investigating ultrafast interfacial PCET dynamics in photon mediated processes.[118,134,138] The challenges are severe, but the rewards for learning how to harness PCET processes in photocatalysis based clean energy generation make the effort essential.

6. Acknowledgments

The authors thank S. Hammes-Schiffer, J. Coe, Y. Matsumoto, A. Nilsson, and O. Prezhdo for helpful discussions; A. Bard for providing the template for Figure 1; K. Onda, B. Li, M. Feng, X. Cui, J. Yang, and K. Jordan for their contributions to the experimental and theoretical studies of ultrafast PCET; and ARO Grant W911NF-07-1-0052, the DoD MURI program under Grant DAAD19-01-1-0619, and NSF Grant CHE-0650756 for financial support. Some of the calculations reported in this work were performed in the Environmental Molecular Sciences Laboratory at the Pacific Northwest National Laboratory, a user facility sponsored by the DOE Office of Biological and Environmental Research.

7. References

(1) Cukier, R. I.; Nocera, D. G. *Annu. Rev. Phys. Chem.* **1998**, *49*, 337.
(2) Huynh, M. H. V.; Meyer, T. J.; White, P. S. *J. Chem. Am. Soc.* **1999**, *121*, 4530.
(3) Hammes-Schiffer, S. *Acc. Chem. Res.* **2001**, *34*, 273.
(4) Hammes-Schiffer, S. *Acc. Chem. Res.* **2009**, *42*, 1881.
(5) Shibata, M.; Kandori, H. *Biochemistry* **2005**, *44*, 7406.
(6) Shibata, M.; Yamashita, H.; Uchihashi, T.; Kandori, H.; Ando, T. *Nat. Nanotechnol.* **2010**, *5*, 208.
(7) McEvoy, J. P.; Brudvig, G. W. *Chem. Rev.* **2006**, *106*, 4455.
(8) Rossmeisl, J.; Skúlason, E.; Björketun, M. E.; Tripkovic, V.; Nørskov, J. K. *Chem. Phys. Lett.* **2008**, *466*, 68.
(9) Santos, E.; Pötting, K.; Schmickler, W. *Faraday Discuss.* **2009**, *140*, 209.
(10) Santos, E.; Lundin, A.; Pötting, K.; Quaino, P.; Schmickler, W. *J. Solid State Electrochem.* **2009**, *13*, 1101.
(11) Fujishima, A.; Zhang, X.; Tryk, D. A. *Surf. Sci. Rep.* **2008**, *63*, 515.
(12) Indrakanti, V. P.; Kubicki, J. D.; Schobert, H. H. *Energy Environ. Sci.* **2009**, *2*, 745.
(13) Hoffmann, M. R.; Martin, S. T.; Choi, W.; Bahnemann, D. W. *Chem. Rev.* **1995**, *95*, 69.
(14) Bovensiepen, U.; Gahl, C.; Stähler, J.; Bockstedte, M.; Meyer, M.; Baletto, F.; Scandolo, S.; Zhu, X. Y.; Rubio, A.; Wolf, M. *J. Phys. Chem. C* **2009**, *113*, 979.
(15) Bard, A. J. *J. Am. Chem. Soc.* **2010**, *132*, 7559.
(16) Nelsen, S. F.; Thompson-Colon, J. A.; Kirste, B.; Rosenhouse, A.; Kaftory, M. *J. Am. Chem. Soc.* **1987**, *109*, 7128.
(17) Salvador, P. *J. Phys. Chem. C* **2007**, *111*, 17038.
(18) Santos, E.; Lundin, A.; Pötting, K.; Quaino, P.; Schmickler, W. *Phys. Rev. B* **2009**, *79*, 235436.
(19) Bartels, L.; Meyer, G.; Rieder, K.-H.; Velic, D.; Knoesel, E.; Hotzel, A.; Wolf, M.; Ertl, G. *Phys. Rev. Lett.* **1998**, *80*, 2004.
(20) Fohlisch, A.; Feulner, P.; Hennies, F.; Fink, A.; Menzel, D.; Sanchez-Portal, D.; Echenique, P. M.; Wurth, W. *Nature* **2005**, *436*, 373.
(21) Ogawa, S.; Nagano, H.; Petek, H. *Phys. Rev. Lett.* **1999**, *82*, 1931.
(22) Borisov, A. G.; Gauyacq, J. P.; Kazansky, A. K.; Chulkov, E. V.; Silkin, V. M.; Echenique, P. M. *Phys. Rev. Lett.* **2001**, *86*, 488.
(23) Zhao, J.; Li, B.; Onda, K.; Feng, M.; Petek, H. *Chem. Rev.* **2006**, *106*, 4402.
(24) Garrett, B. C.; Dixon, D. A.; Camaioni, D. M.; Chipman, D. M.; Johnson, M. A.; Jonah, C. D.; Kimmel, G. A.; Miller, J. H.; Rescigno, T. N.; Rossky, P. J.; Xantheas, S. S.; Colson, S. D.; Laufer, A. H.; Ray, D.; Barbara, P. F.; Bartels, D. M.; Becker, K. H.; Bowen, H.; Bradforth, S. E.; Carmichael, I.; Coe, J. V.; Corrales, L. R.; Cowin, J. P.; Dupuis, M.; Eisenthal, K. B.; Franz, J. A.; Gutowski, M. S.; Jordan, K. D.; Kay, B. D.; LaVerne, J. A.; Lymar, S. V.; Madey, T. E.; McCurdy, C. W.; Meisel, D.; Mukamel, S.; Nilsson, A. R.; Orlando, T. M.; Petrik, N. G.; Pimblott, S. M.; Rustad, J. R.; Schenter, G. K.; Singer, S. J.; Tokmakoff, A.; Wang, L. S.; Wittig, C.; Zwier, T. S. *Chem. Rev.* **2005**, *105*, 355.
(25) Grimminger, J.; Schmickler, W. *Chem. Phys.* **2007**, *334*, 8.
(26) Marcus, R. A. *J. Chem. Phys.* **1965**, *43*, 679.
(27) Zhao, J.; Pontius, N.; Winkelmann, A.; Sametoglu, V.; Kubo, A.; Borisov, A. G.; Sanchez-Portal, D.; Silkin, V. M.; Chulkov, E. V.; Echenique, P. M.; Petek, H. *Phys. Rev. B* **2008**, *78*, 085419.
(28) Borisov, A. G.; Sametoglu, V.; Winkelmann, A.; Kubo, A.; Pontius, N.; Zhao, J.; Silkin, V. M.; Gauyacq, J. P.; Chulkov, E. V.; Echenique, P. M.; Petek, H. *Phys. Rev. Lett.* **2008**, *101*, 266801.
(29) Petek, H.; Weida, M. J.; Nagano, H.; Ogawa, S. *Science* **2000**, *288*, 1402.
(30) Sametoglu, V. Ph.D. Thesis, University of Pittsburgh, 2009.
(31) Hammes-Schiffer, S.; Soudackov, A. V. *J. Phys. Chem. B* **2008**, *112*, 14108.
(32) Venkataraman, C.; Soudackov, A. V.; Hammes-Schiffer, S. *J. Phys. Chem. C* **2008**, *112*, 12386.
(33) Navrotskaya, I.; Soudackov, A. V.; Hammes-Schiffer, S. *J. Chem. Phys.* **2008**, *128*, 244712.
(34) Costentin, C. *Chem. Rev.* **2008**, *108*, 2145.
(35) Bovensiepen, U. *Prog. Surf. Sci.* **2005**, *78*, 87.
(36) Stähler, J.; Bovensiepen, U.; Meyer, M.; Wolf, M. *Chem. Soc. Rev.* **2008**, *37*, 2180.
(37) Gouy, G. *J. Phys. (Paris)* **1910**, *9*, 457.
(38) Chapman, D. L. *Philos. Mag.* **1913**, *6*, 475.
(39) Mott, N. F.; Watts-Tobin, R. J. *Electrochim. Acta* **1961**, *4*, 79.
(40) Gomer, R.; Tryson, G. *J. Chem. Phys.* **1977**, *66*, 4413.
(41) Taylor, C. D.; Wasileski, S. A.; Filhol, J.-S.; Neurock, M. *Phys. Rev. B* **2006**, *73*, 165402.
(42) Bockris, J. O. M.; Reddy, A. K. N.; Gamboa-Aldeco, M. *Modern Electrochemistry*; Kluwer Academic/Plenum Publishers: New York, 2000.
(43) Israelachvili, J. N. *Intermolecular and Surface Forces*, 2nd ed.; Academic Press Inc.: London, 1997.
(44) Taylor, C. D.; Neurock, M. *Curr. Opin. Solid State Mater. Sci.* **2005**, *9*, 49.
(45) Kumar, N.; Neogi, S.; Kent, P. R. C.; Bandura, A. V.; Kubicki, J. D.; Wesolowski, D. J.; Cole, D.; Sofo, J. O. *J. Phys. Chem. C* **2009**, *113*, 13732.
(46) Eftekhari-Bafrooei, A.; Borguet, E. *J. Am. Chem. Soc.* **2009**, *131*, 12034.
(47) Bagus, P. S.; Käfer, D.; Witte, G.; Wöll, C. *Phys. Rev. Lett.* **2008**, *100*, 126101.
(48) *Chemical Bonding at Surfaces and Interfaces*, 1st ed.; Nilsson, A., Pettersson, L. G. M., Nørskov, J. K., Eds.; Elsevier: Amsterdam, 2008.
(49) García-Lastra, J. M.; Rostgaard, C.; Rubio, A.; Thygesen, K. S. *Phys. Rev. B* **2009**, *80*, 245427.
(50) Lang, N. D.; Kohn, W. *Phys. Rev. B* **1973**, *7*, 3541.
(51) Lang, N. D.; Williams, A. R. *Phys. Rev. B* **1978**, *18*, 616.
(52) Echenique, P. M.; Pendry, J. B. *Prog. Surf. Sci.* **1990**, *32*, 111.
(53) Chulkov, E. V.; Silkin, V. M.; Echenique, P. M. *Surf. Sci.* **1999**, *437*, 330.
(54) Tsirkin, S.; Eremeev, S.; Chulkov, E. *Phys. Solid State* **2010**, *52*, 188.
(55) Echenique, P. M.; Berndt, R.; Chulkov, E. V.; Fauster, T.; Goldmann, A.; Höfer, U. *Surf. Sci. Rep.* **2004**, *52*, 219.
(56) Ge, N.-H.; Wong, C. M.; Lingle, R. L., Jr.; McNeill, J. D.; Gaffney, K. J.; Harris, C. B. *Science* **1998**, *279*, 202.
(57) Fauster, T.; Weinelt, M.; Höfer, U. *Prog. Surf. Sci.* **2007**, *82*, 224.
(58) Neaton, J. B.; Hybertsen, M. S.; Louie, S. G. *Phys. Rev. Lett.* **2006**, *97*, 216405.
(59) Thygesen, K. S.; Rubio, A. *Phys. Rev. Lett.* **2009**, *102*, 046802.
(60) Silkin, V. M.; Zhao, J.; Guinea, F.; Chulkov, E. V.; Echenique, P. M.; Petek, H. *Phys. Rev. B* **2009**, *80*, 121408.

(61) Petek, H.; Feng, M.; Zhao, J. In *Current-driven phenomena in nanoelectronics*; Seideman, T., Ed.; World Scientific: 2010.
(62) Chiang, T. C.; Kaindl, G.; Mandel, T. *Phys. Rev. B* **1986**, *33*, 695.
(63) Fernandez Torrente, I.; Franke, K. J.; Pascual, J. I. *J. Phys.: Condens. Matter* **2008**, 184001.
(64) Achilli, S.; Trioni, M. I.; Chulkov, E. V.; Echenique, P. M.; Sametoglu, V.; Pontius, N.; Winkelmann, A.; Kubo, A.; Zhao, J.; Petek, H. *Phys. Rev. B* **2009**, *80*, 245419.
(65) Borisov, A. G.; Kazansky, A. K.; Gauyacq, J. P. *Surf. Sci.* **1999**, *430*, 165.
(66) Petek, H.; Weida, M. J.; Nagano, H.; Ogawa, S. *Surf. Sci.* **2000**, *451*, 22.
(67) Fischer, N.; Schuppler, S.; Fauster, T.; Steinmann, W. *Surf. Sci.* **1994**, *314*, 89.
(68) Ishii, H.; Sugiyama, K.; Ito, E.; Seki, K. *Adv. Mater.* **1999**, *11*, 605.
(69) Breitholtz, M.; Chis, V.; Hellsing, B.; Lindgren, S. Å.; Wallden, L. *Phys. Rev. B* **2007**, *75*, 155403.
(70) Echenique, P. M.; Pendry, J. B. *J. Phys. C* **1978**, *11*, 2065.
(71) Wilhelm, F.; Schmickler, W.; Nazmutdinov, R. R.; Spohr, E. *J. Phys. Chem. C* **2008**, *112*, 10814.
(72) Ohwaki, T.; Yamashita, K. *J. Electroanal. Chem.* **2001**, *504*, 71.
(73) Tissandier, M. D.; Cowen, K. A.; Feng, W. Y.; Gundlach, E.; Cohen, M. H.; Earhart, A. D.; Coe, J. V.; Tuttle, T. R. *J. Phys. Chem. A* **1998**, *102*, 7787.
(74) Donald, W. A.; Leib, R. D.; O'Brien, J. T.; Williams, E. R. *Chem.—Eur. J.* **2009**, *15*, 5926.
(75) Wasileski, S.; Taylor, C.; Neurock, M. Topics in Applied Physics, In *Device and Materials Modeling in PEM Fuel Cells*; Paddison, S. J., Promislow, K. S., Eds.; Springer: 2009, Volume 113/2009, 551−574, DOI: 10.1007/978-0-387-78691-9_21.
(76) Headrick, J. M.; Diken, E. G.; Walters, R. S.; Hammer, N. I.; Christie, R. A.; Cui, J.; Myshakin, E. M.; Duncan, M. A.; Johnson, M. A.; Jordan, K. D. *Science* **2005**, *308*, 1765.
(77) Marx, D. *ChemPhysChem* **2006**, *7*, 1848.
(78) Hartnig, C.; Koper, M. T. M. *J. Phys. Chem. B* **2004**, *108*, 3824.
(79) Otani, M.; Hamada, I.; Sugino, O.; Morikawa, Y.; Okamoto, Y.; Ikeshoji, T. *J. Phys. Soc. Jpn.* **2008**, *77*, 024802.
(80) Iwasita, T.; Nart, F. C. *Prog. Surf. Sci.* **1997**, *55*, 271.
(81) Mrozek, M. F.; Weaver, M. J. *J. Am. Chem. Soc.* **200**, *122*, 150.
(82) Kawata, S.; Osawa, M. In *Near-Field Optics and Surface Plasmon Polaritons*; Springer: Berlin/Heidelberg, 2001; Vol. 81.
(83) Schultz, Z. D.; Shaw, S. K.; Gewirth, A. A. *J. Am. Chem. Soc.* **2005**, *127*, 15916.
(84) He, Y.; Borguet, E. *Angew. Chem., Int. Ed.* **2007**, *46*, 6098.
(85) Watanabe, K.; Sawabe, K.; Matsumoto, Y. *Phys. Rev. Lett.* **1996**, *76*, 1751.
(86) Matsumoto, Y.; Gruzdkov, Y. A.; Watanabe, K.; Sawabe, K. *J. Chem. Phys.* **1996**, *105*, 4775.
(87) Matsumoto, Y. *Bull. Chem. Soc. Jpn.* **2007**, *80*, 842.
(88) Yoshinobu, J.; Ogasawara, H.; Kawai, M. *Phys. Rev. Lett.* **1995**, *75*, 2176.
(89) Öström, H.; Ogasawara, H.; Näslund, L. Å.; Pettersson, L. G. M.; Nilsson, A. *Phys. Rev. Lett.* **2006**, *96*, 146104.
(90) Yamaguchi, D.; Matsumoto, T.; Watanabe, K.; Takagi, N.; Matsumoto, Y. *Phys. Chem. Chem. Phys.* **2006**, *8*, 179.
(91) Öström, H.; Triguero, L.; Nyberg, M.; Ogasawara, H.; Pettersson, L. G. M.; Nilsson, A. *Phys. Rev. Lett.* **2003**, *91*, 046102.
(92) Öström, H.; Ogasawara, H.; Näslund, L. Å.; Andersson, K.; Pettersson, L. G. M.; Nilsson, A. *J. Chem. Phys.* **2007**, *127*, 144702.
(93) Demuth, J. E.; Ibach, H.; Lehwald, S. *Phys. Rev. Lett.* **1978**, *40*, 1044.
(94) Raval, R.; Parker, S. F.; Chesters, M. A. *Surf. Sci.* **1993**, *289*, 227.
(95) Zhou, X.-L.; Zhu, X.-Y.; White, J. M. *Surf. Sci. Rep.* **1991**, *13*, 73.
(96) Ho, W. *J. Phys. Chem.* **1996**, *100*, 13050.
(97) *Laser Spectroscopy and Photochemistry on Metal Surfaces*; Dai, H.-L., Ho, W., Eds.; World Scientific: Singapore, 1995; Vol. 5.
(98) *Dynamics at Solid State Surfaces and Interfaces*; Bovensiepen, U., Petek, H., Wolf, M., Eds.; Wiley-VCH Verlag Gmbh & Co.: Weinheim, 2010; Vol. 1, Current developments.
(99) Petek, H.; Nagano, H.; Weida, M. J.; Ogawa, S. *J. Phys. Chem. B* **2001**, *105*, 6767.
(100) Wöll, C.; Weiss, K.; Bagus, P. S. *Chem. Phys. Lett.* **2000**, *332*, 553.
(101) Borisov, A. G.; Kazansky, A. K.; Gauyacq, J. P. *Phys. Rev. B* **1999**, *59*, 10935.
(102) Ushiyama, H.; Takatsuka, K. *Angew. Chem., Int. Ed.* **2007**, *46*, 587.
(103) Watanabe, K.; Matsumoto, Y. *Faraday Discuss.* **2000**, *117*, 203.
(104) Odelius, M.; Ogasawara, H.; Nordlund, D.; Fuchs, O.; Weinhardt, L.; Maier, F.; Umbach, E.; Heske, C.; Zubavichus, Y.; Grunze, M.; Denlinger, J. D.; Pettersson, L. G. M.; Nilsson, A. *Phys. Rev. Lett.* **2005**, *94*, 227401.
(105) Ito, M. *Surf. Sci. Rep.* **2008**, *63*, 329.
(106) Salmeron, M.; Bluhm, H.; Tatarkhanov, M.; Ketteler, G.; Shimizu, T. K.; Mugarza, A.; Deng, X.; Herranz, T.; Yamamoto, S.; Nilsson, A. *Faraday Discuss.* **2009**, *141*, 221.
(107) Feibelman, P. J. *Phys. Today* **2010**, *63*, 34.
(108) Ogasawara, H.; Brena, B.; Nordlund, D.; Nyberg, M.; Pelmenschikov, A.; Pettersson, L. G. M.; Nilsson, A. *Phys. Rev. Lett.* **2002**, *89*, 276102.
(109) Michaelides, A.; Ranea, V. A.; de Andres, P. L.; King, D. A. *Phys. Rev. Lett.* **2003**, *90*, 216102.
(110) Meng, S.; Wang, E. G.; Gao, S. *Phys. Rev. B* **2004**, *69*, 195404.
(111) Schiros, T.; Takahashi, O.; Andersson, K. J.; Öström, H.; Pettersson, L. G. M.; Nilsson, A.; Ogasawara, H. *J. Chem. Phys.* **2010**, *132*, 094701.
(112) Backus, E. H. G.; Grecea, M. L.; Kleyn, A. W.; Bonn, M. *J. Phys. Chem. B* **2007**, *111*, 6141.
(113) Mehlhorn, M.; Carrasco, J.; Michaelides, A.; Morgenstern, K. *Phys. Rev. Lett.* **2009**, *103*, 026101.
(114) Fenter, P.; Sturchio, N. C. *Prog. Surf. Sci.* **2004**, *77*, 171.
(115) Ketteler, G.; Yamamoto, S.; Bluhm, H.; Andersson, K.; Starr, D. E.; Ogletree, D. F.; Ogasawara, H.; Nilsson, A.; Salmeron, M. *J. Phys. Chem. C* **2007**, *111*, 8278.
(116) Onda, K.; Li, B.; Zhao, J.; Jordan, K. D.; Yang, J.; Petek, H. *Science* **2005**, *308*, 1154.
(117) Onda, K.; Li, B.; Zhao, J.; Petek, H. *Surf. Sci.* **2005**, *593*, 32.
(118) Li, B.; Zhao, J.; Onda, K.; Jordan, K. D.; Yang, J.; Petek, H. *Science* **2006**, *311*, 1436.
(119) Onda, K.; Li, B.; Petek, H. *Phys. Rev. B* **2004**, *70*, 045415.
(120) Chiodo, L.; García-Lastra, J. M.; Iacomino, A.; Ossicini, S.; Zhao, J.; Petek, H.; Rubio, A. *Phys. Rev. B* **2010**, *82*, 045207.
(121) Gopel, W.; Anderson, J. A.; Frankel, D.; Jaehnig, M.; Phillips, K.; Schafer, J. A.; Rocker, G. *Surf. Sci.* **1984**, *139*, 333.
(122) Minato, T.; Sainoo, Y.; Kim, Y.; Kato, H. S.; Aika, K.-i.; Kawai, M.; Zhao, J.; Petek, H.; Huang, T.; He, W.; Wang, B.; Wang, Z.; Zhao, Y.; Yang, J.; Hou, J. G. *J. Chem. Phys.* **2009**, *130*, 124502.
(123) Papageorgiou, A. C.; Beglitis, N. S.; Pang, C. L.; Teobaldi, G.; Cabailh, G.; Chen, Q.; Fisher, A. J.; Hofer, W. A.; Thornton, G. *Proc. Natl. Acad. Sci.* **2010**, *107*, 2391.
(124) Liu, L.-M.; Crawford, P.; Hu, P. *Prog. Surf. Sci.* **2009**, *84*, 155.
(125) Dohnalek, Z.; Lyubinetsky, I.; Rousseau, R. *Prog. Surf. Sci.* **2010**, *85*, 161.
(126) Wendt, S.; Matthiesen, J.; Schaub, R.; Vestergaard, E. K.; Laegsgaard, E.; Besenbacher, F.; Hammer, B. *Phys. Rev. Lett.* **2006**, *96*, 066107.
(127) Zhang, Z.; Bondarchuk, O.; Kay, B. D.; White, J. M.; Dohnálek, Z. *J. Phys. Chem. B* **2006**, *110*, 21840.
(128) Zhang, Z.; Bondarchuk, O.; White, J. M.; Kay, B. D.; Dohnálek, Z. *J. Am. Chem. Soc.* **2006**, *128*, 4198.
(129) Zhao, J.; Li, B.; Jordan, K. D.; Yang, J.; Petek, H. *Phys. Rev. B* **2006**, *73*, 195309.
(130) Machesky, M. L.; Předota, M.; Wesolowski, D. J.; Vlcek, L.; Cummings, P. T.; Rosenqvist, J.; Ridley, M. K.; Kubicki, J. D.; Bandura, A. V.; Kumar, N.; Sofo, J. O. *Langmuir* **2008**, *24*, 12331.
(131) Gahl, C.; Bovensiepen, U.; Frischkorn, C.; Wolf, M. *Phys. Rev. Lett.* **2002**, *89*, 107402.
(132) Prezhdo, O. V.; Duncan, W. R.; Prezhdo, V. V. *Prog. Surf. Sci.* **2009**, *84*, 30.
(133) Prezhdo, O. V.; Rossky, P. J. *J. Chem. Phys.* **1997**, *107*, 5863.
(134) Fischer, S. A.; Duncan, W. R.; Prezhdo, O. V. *J. Am. Chem. Soc.* **2009**, *131*, 15483.
(135) Huber, R.; Moser, J. E.; Grätzel, M.; Wachtveitl, J. *J. Phys. Chem. B* **2002**, *106*, 6494.
(136) Gundlach, L.; Ernstorfer, R.; Willig, F. *Prog. Surf. Sci.* **2007**, *82*, 355.
(137) Zhao, J.; Yang, J.; Petek, H. *Phys. Rev. B* **2009**, *80*, 235416.
(138) Venkataraman, C.; Soudackov, A. V.; Hammes-Schiffer, S. *J. Phys. Chem. C* **2010**, *114*, 487.
(139) Henderson, M. A.; Otero-Tapia, S.; Castro, M. E. *Faraday Discuss.* **1999**, *114*, 313.
(140) Farfan-Arribas, E.; Madix, R. J. *Surf. Sci.* **2003**, *544*, 241.
(141) Indrakanti, V. P.; Schobert, H. H.; Kubicki, J. D. *Energy Fuels* **2009**, *23*, 5247.
(142) Kawai, T.; Sakata, T. *J. Chem. Soc., Chem. Commun.* **1980**, 694.
(143) Micic, O.; Zhang, Y.; Cromack, K. R.; Trifunac, A.; Thurnauer, M. *J. Phys. Chem.* **1993**, *97*, 13284.
(144) Villarreal, T. L.; Gomez, R.; Neumann-Spallart, M.; Alonso-Vante, N.; Salvador, P. *J. Phys. Chem. B* **2004**, *108*, 15172.
(145) Du, M.-H.; Feng, J.; Zhang, S. B. *Phys. Rev. Lett.* **2007**, *98*, 066102.
(146) Silva, C.; Walhout, P. K.; Reid, P. J.; Barbara, P. F. *J. Phys. Chem. A* **1998**, *102*, 5701.
(147) Turi, L. *J. Chem. Phys.* **1999**, *110*, 10364.
(148) Turi, L.; Mosyak, A.; Rossky, P. J. *J. Chem. Phys.* **1997**, *107*, 1970.
(149) Kammrath, A.; Griffin, G. B.; Verlet, J. R. R.; Young, R. M.; Neumark, D. M. *J. Chem. Phys.* **2007**, *126*, 244306.

(150) Tauber, M. J.; Stuart, C. M.; Mathies, R. A. *J. Am. Chem. Soc.* **2004**, *126*, 3414.
(151) Li, B. Ph.D. Thesis, University of Pittsburgh, 2006.
(152) Monnier, R.; Perdew, J. P.; Langreth, D. C.; Wilkins, J. W. *Phys. Rev. B* **1978**, *18*, 656.
(153) Hellman, A.; Razaznejad, B.; Lundqvist, B. I. *J. Chem. Phys.* **2004**, *120*, 4593.
(154) Fujishima, A.; Honda, K. *Nature* **1972**, *238*, 37.
(155) Varghese, O. K.; Paulose, M.; LaTempa, T. J.; Grimes, C. A. *Nano Lett.* **2009**, *9*, 731.
(156) Krausz, F.; Ivanov, M. *Rev. Mod. Phys.* **2009**, *81*, 163.
(157) Cavalieri, A. L.; Muller, N.; Uphues, T.; Yakovlev, V. S.; Baltuska, A.; Horvath, B.; Schmidt, B.; Blumel, L.; Holzwarth, R.; Hendel, S.; Drescher, M.; Kleineberg, U.; Echenique, P. M.; Kienberger, R.; Krausz, F.; Heinzmann, U. *Nature* **2007**, *449*, 1029.
(158) Nilsson, A.; Pettersson, L. G. M. *Surf. Sci. Rep.* **2004**, *55*, 49.
(159) Arnolds, H.; Bonn, M. *Surf. Sci. Rep.* **2010**, *65*, 45.

CR1001595